

Impact of Primordial Ultracompact Minihaloes on the Intergalactic Medium and First Structure Formation

Dong Zhang^{1*}

¹*Department of Astronomy, Ohio State University, 140 W. 18th Ave., Columbus, OH 43210, USA*

10 August 2011

ABSTRACT

The effects of dark matter annihilation on the evolution of intergalactic medium (IGM) in the early Universe can be more important if dark matter structure is more concentrated. Ultracompact Minihaloes (UCMHs), which formed by dark matter accretion onto primordial black holes (PBHs) or initial dark matter overdensity produced by the primordial density perturbation, provide a new type of compact dark matter structure to ionize and heat the IGM after matter-radiation equality z_{eq} , which is much earlier than the formation of the first cosmological dark halo structure and later first stars. We show that dark matter annihilation density contributed by UCMHs can totally dominated over the homogenous dark matter annihilation background even for a tiny UCMH fraction $f_{\text{UCMH}} = \Omega_{\text{UCMH}}(z_{\text{eq}})/\Omega_{\text{DM}} \geq 10^{-15}(1+z)^2(m_\chi c^2/100 \text{ GeV})^{-2/3}$ with a standard thermal relic dark matter annihilation cross section, and provide a new gamma-ray background in the early Universe. UCMH annihilation becomes important to the IGM evolution approximately for $f_{\text{UCMH}} > 10^{-6}(m_\chi c^2/100 \text{ GeV})$. The IGM ionization fraction x_{ion} and gas temperature T_{m} can be increased from the recombination residual $x_{\text{ion}} \sim 10^{-4}$ and adiabatically cooling $T_{\text{m}} \propto (1+z)^2$ in the absence of energy injection, to the highest value of $x_{\text{ion}} \sim 0.1$ and $T_{\text{m}} \sim 5000 \text{ K}$ at $z \geq 10$ for the upper bound UCMH abundance constrained by the cosmic microwave background optical depth.

A small fraction of UCMHs are seeded by PBHs. The X-ray emission from gas accretion onto PBHs may totally dominated over dark matter annihilation and become the main cosmic ionization source for a PBH abundance $f_{\text{PBH}} = \Omega_{\text{PBH}}/\Omega_{\text{DM}} \gg 10^{-11}$ (10^{-12}) with the PBH mass $M_{\text{PBH}} \sim 10^{-6}M_\odot$ (10^2M_\odot). However, the constraints of gas accretion rate and X-ray absorption by the baryon accumulation within the UCMHs and accretion feedback show that X-ray emission can only be a promising source much later than UCMH annihilation at $z < z_m \ll 1000$, where z_m depends on the masses of PBHs, their host UCMHs, and the dark matter particles. Also, UCMH radiation including both annihilation and X-ray emission can significantly suppress the low mass first baryonic structure formation. The effects of UCMHs radiation on the baryonic structure evolution are quite small for the gas temperature after virialization, but more significant to enhance the gas chemical quantities such as the ionization fraction and molecular hydrogen abundance in the baryonic objects.

Key words: intergalactic medium — dark matter — cosmology: theory — early Universe — galaxies: structure

1 INTRODUCTION

Ultracompact Minihaloes (UCMHs) are primordial dark matter structures which formed by dark matter accreting onto primordial black holes (PBHs) after matter-radiation equality $z_{\text{eq}} \sim 3100$, or direct collapsed onto an initial

dark matter overdensity produced by small density perturbation before z_{eq} , e.g., in several Universe phase transition epochs (Mack et al. 2007; Ricotti & Gould 2009). If the density perturbation in the early Universe exceed a critical value $\delta_c = (\delta\rho/\rho)_c \sim 1/3$, this region becomes gravitationally unstable and directly collapse to form a PBH (Hawking 1971; Carr & Hawking 1974; see Khlopov 2010 for a review and references therein). PBHs which form with

* dzhang@astronomy.ohio-state.edu

a sufficient high mass $\geq 10^{16}$ gram do not evaporate but begin to grow by accreting the surrounding dark matter and form a compact dark matter halo, which will grow by two orders of magnitude in mass during the matter dominated era (Mack et al. 2007). These haloes are so-called Ultracompact Minihaloes (UCMHs), or say Primordially-Laid Ultracompact Minihaloes (PLUMs). On the other hand, small density perturbation in the early Universe $10^{-3} < \delta < \delta_c$ will form a compact dark matter overdensity instead of a PBH. Such an overdense cloud can also seed the formation of UCMHs (Ricotti & Gould 2009; Scott & Sivertsson 2009; Josan & Green 2010). Note that the initial density perturbations from inflation were just $\delta \sim 10^{-4} - 10^{-5}$, it is proposed UCMHs are far more viable to form by accreting onto dark matter overdensity, which requires a much lower perturbation threshold than PBHs. Also, the UCMHs seeded by primordial overdensities have a different profile with those seeded by PBHs (Bertschinger 1985; Mack et al. 2007).

UCMHs have been recently proposed as a new type of non-baryonic massive compact gravitational object (MA-CHO; Ricotti & Gould 2009) as well as gamma-ray and neutrino source (Scott & Sivertsson 2009). UCMHs could produce a microlensing lightcurve which can be distinguished from that of a “point-like” object such as a star or brown dwarf, thus become a promising new target for microlensing searches. Moreover, the abundance of UCMHs can be constrained by the observation of the Milky Way gamma-ray flux and the extragalactic gamma-ray background, although this constraint is still very uncertain based on today’s data (Lacki & Beacom 2010; Josan & Green 2010; Saito & Shirai 2011). Since we know the growth of an isolate UCMH as a function of redshift (Mack et al. 2007), we can natively trace the fraction of UCMHs back to very high redshift without considering mergers and tidal destruction. Until now, most of the works on UCMHs focus on the properties of the nearby UCMHs at $z < 1$. Another important question which has barely been discussed is that, what are the consequences of UCMH radiation at very high redshift, since UCMHs are the “remnants” originally from the early Universe? As the sources of heating and ionization before the first structure, stars and galaxies, sufficient UCMHs may play important roles to change the chemical and thermal history of the early Universe. Our main purpose in this paper is to investigate the impacts of UCMH emission on the intergalactic medium (IGM) in the Universe reionization era, and the following first baryon structure formation and evolution.

The process of reionization of all hydrogen atoms in the IGM would have been completed at redshift $z \approx 6$ (e.g., Becker et al. 2001; Fan et al. 2002). However, much earlier ionization at $z > 6$ is implied by the WMAP observation (e.g., Dunkley et al. 2009; Komatsu et al. 2009). It is commonly suggested that the possible contributions to the high redshift reionization between approximately $6 < z < 20$ are the first baryonic objects to produce significant ultraviolet light, early (Pop III and Pop II) stars, and old quasars (Barkana & Loeb 2007; Wise & Abel 2008; Volonteri & Gnedin 2009; Meiksin 2009). However, it is still unclear whether quasars and first stars were sufficiently efficiency to reionize the universe. Dark matter, on the other hand, is suggested to be the exotic source of ionization and heating at high redshift due to its self-annihilation or decay. It is usually proposed that weakly interacting massive parti-

cles (WIMPs) provide a compelling solution to identify the dark matter component. The mass of the dark matter particles m_χ , and the average annihilation cross section $\langle\sigma v\rangle$ are the two crucial parameters to affect the ionizing and heating processes. Under the thermal relic assumption that the cross section $\langle\sigma v\rangle \approx 3 \times 10^{-26} \text{ cm}^3 \text{ s}^{-1}$ to match the observed $\Omega_{\text{DM}} h^2 \approx 0.110$, most previous studies showed that the effects of homogenous dark matter background annihilation or decay on the high-redshift IGM are expected to be important only for light dark matter $m_\chi c^2 \leq 1 \text{ GeV}$ or sterile neutrinos (e.g., Hansen & Haiman 2004; Pierpaoli 2004; Mapelli & Ferrara 2005; Belotsky et al. 2005; Zhang et al. 2006; Mapelli et al. 2006; Ripamonti et al. 2007a,b; Chluba 2010). The annihilation flux would be enhanced only after the formation of the first dark objects $z < 60$, as dark matter become more clumpy (e.g., Chuzhoy 2008; Natarajan & Schwarz 2008, 2009, 2010; Belikov & Hooper 2009, 2010). However, in our case, as dark matter is more concentrated in UCMHs which are significantly denser than the homogenous dark matter background, WIMP dark matter annihilation within UCMHs may become powerful gamma-ray source dominated over the homogenous background annihilation, even though UCMHs are very rare.

A small fraction of UCMHs are seeded by PBHs (Mack et al. 2007). In this paper we call these UCMHs as PBH host UCMHs. Since PBH abundance is still uncertain for a broad range of PBH mass (Josan & Green 2009; Carr et al. 2010), we only give a qualitative estimate that the abundance of PBH host UCMHs should be much less than other UCMHs. For PBH host UCMHs, the X-ray emission from the accreting baryonic gas flows onto PBHs may totally dominated over dark matter annihilation within the host UCMH, since the Eddington luminosity is several orders of magnitude brighter than that of annihilation from the host UCMH, and the photoionization cross section for hydrogen or helium is much larger than the Klein-Nishina or pair production cross section for energetic gamma-rays. It is very difficult for a “naked” PBH to reach a sufficient high accretion rate in the IGM environment, (Barrow & Silk 1979; Carr 1981; Gendin et al. 1995; Miller & Ostriker 2001; Ricotti 2007; Ricotti et al. 2008; Mack & Wesley 2008), but the situation will be quite different if PBHs are surrounded by UCMHs. The accretion rate and X-ray luminosity of baryons can change significantly when the effects of a growth UCMH is involved (Ricotti 2007; Ricotti et al. 2008). However, it is possible that the gas is heated and piles up around the PBH if the host UCMH is sufficiently massive. Also, the accretion feedback such as outflows or radiation pressure prevent gas from being totally eaten by the PBH immediately, if the gas accretion rate significantly exceeds the Eddington limit. As a consequence, the gas density and temperature within the UCMH may be significantly higher than the cosmic universal gas density, and the X-ray emission is totally absorb in the UCMH, but reradiate basically in the infrared band. In this paper we will give criteria for X-ray emission escaping from the host UCMH to ionize the IGM. Also we will compare the importance of X-ray emission from PBH host UCMHs and dark matter annihilation from total UCMHs in the early Universe, depending on the abundance of both total UCMHs and PBH host UCMHs.

Another topic related to the UCMH radiation is that, the formation and evolution history of the first baryonic

structure can be changed by UCMH radiation. Previous studies showed that the annihilation or decay of the extended distributed dark matter in the first structure both change the gas temperature and the chemical properties such as the abundance of molecular coolants such as H_2 and HD (Biermann & Kusenko 2006; Stasielak et al. 2007; Ripamonti et al. 2007b). Higher coolants abundance helps to decrease the gas temperature and favors an early collapse of the baryon gas inside the halo, but dark matter energy injection delays this collapsing process. It is still under debate whether dark matter annihilation or decay inside the dark halo will promote or suppress the first structure formation. Nevertheless, it is concluded that either the promotion or suppression effect is quite small for most dark matter models, as the change of gas temperature in a virialized halo for various dark matter models is small. If the first large scale dark haloes contain UCMHs, these UCMHs can inject more annihilation energy into the halo than the first dark haloes, and potentially play more important role to change the properties of the first haloes than the extended distributed dark matter in haloes. Moreover, X-ray emission which comes from PBHs also suppress the formation of the first baryonic objects. Therefore it is also worthwhile to study the effects of UCMH radiation on the first structure formation and evolution.

This paper is organized as follows. In Section 2, we calculate the dark matter annihilation luminosity from UCMHs, and the X-ray emission from PBH gas accretion. We emphasize on the importance of UCMH annihilation compared to the homogenous dark matter background annihilation, and focus on the physical reasons that whether and when the X-ray emission from PBHs becomes more important than the UCMH annihilation in the early Universe. In Section 3 we discuss the gas heating and ionization process by the two types of UCMH radiation from $z \sim 1000$ to 10, and investigate the impact of UCMH radiation on the IGM evolution. Next in Section 4 we show the influences of UCMH radiation on the first baryonic structure formation and evolution. The main results of this paper are given in Sections 3 and 4. In Section 5 we discuss the importance of UCMHs in the reionization era, the effects of a single massive UCMH in the first baryonic structure, as well as other secondary effects. Reader could skip this section and directly go to Section 6, which presents the conclusions. In this paper we do not consider dark matter decay, which should have similar consequences as the annihilation process. Also we fix the annihilation cross section to be thermal relic $\langle\sigma v\rangle = 3 \times 10^{-26} \text{ cm}^3 \text{ s}^{-1}$, although much larger cross section $\langle\sigma v\rangle = 3 \times 10^{-24} \text{ cm}^3 \text{ s}^{-1}$ to $10^{-20} \text{ cm}^3 \text{ s}^{-1}$ is proposed in the hope of explaining the reported Galactic cosmic ray anomalies as the results of dark matter annihilation (e.g., Chang et al. 2008; Abdo et al. 2009; Aharonian et al. 2008). A larger cross section with the same dark matter particle mass m_χ can have higher luminosity and more significant influence on ionizing and heating the early Universe. Table 1 gives the notation and definition of some quantities in this paper.

2 RADIATION FROM UCMHS

In this section we discuss two types of energy emission from UCMHs in the early Universe: dark matter annihilation, and

X-ray emission from the accreting baryonic gas onto PBHs. As mentioned in Section 1, the second type of emission is related to a small fraction of UCMHs, which host PBHs. Generally we still call the second type of energy emission as UCMH radiation, that is because a PBH is always located in the center of its host UCMH and belong to a PBH-UCMH system.

2.1 Dark Matter Annihilation

Dark matter annihilation luminosity of nearby UCMHs ($z = 0$) is calculated recently (Scott & Sivertsson 2009; Lacki & Beacom 2010; Josan & Green 2010; Saito & Shirai 2011). We assume that UCMHs stop growing at $z \approx 10$ when the structure formation progressed deeply to prevent dark matter from further accreting. Now we calculate the annihilation luminosity as the function of redshift in the early Universe before $z \approx 10$, and compare the result to the homogenous background annihilation. The mass of the UCMHs accreted by dark matter radial infall is given by (Mack et al. 2007; Ricotti & Gould 2009; Scott & Sivertsson 2009; Josan & Green 2010)

$$m_h(z) = \delta m \left(\frac{1 + z_{\text{eq}}}{1 + z} \right), \quad (1)$$

where $z_{\text{eq}} \approx 3100$ is the redshift of matter-radiation equality, and δm is the mass of initial dark matter overdensity. The density profile in an UCMH $\propto r^{-\alpha}$ can be written as

$$\rho_\chi(r, z) = \frac{(3 - \alpha)m_h(z)}{4\pi R_h^{3-\alpha} r^\alpha}, \quad (2)$$

where the factor $(3 - \alpha)/4\pi$ in equation (2) is obtained by normalizing the total mass inside the maximum halo extent radius R_h as δm , and R_h is calculated by

$$R_h(z) \approx 0.019 \text{ pc} \left(\frac{1000}{1 + z} \right) \left(\frac{m_h(z)}{M_\odot} \right)^{1/3}. \quad (3)$$

Dark matter annihilation reduces the density in the inner region of an UCMH, and makes the density in this region to be flat. Following Ullio et al. (2002) the UCMH power-law density distribution is truncated at the maximum density

$$\rho(r_{\text{cut}}) = \rho_{\text{max}} = \frac{m_\chi}{\langle\sigma v\rangle(t - t_i)}, \quad (4)$$

where $t \approx \frac{2}{3}(1 + z)^{-3/2}(\Omega_{\text{m},0})^{-1/2}H_0^{-1}$ is the age of the Universe at a certain redshift z , and $t_i \approx 77 \text{ kyr}$ is the initial age at z_{eq} . Thus the total dark matter annihilation luminosity within the UCMH can be calculated as

$$\begin{aligned} L_{\text{ann}} &= \int_0^{R_h} 2\pi r^2 n_\chi^2(r) \langle\sigma v\rangle m_\chi c^2 dr \\ &= \frac{2\pi c^2}{3} \left(\frac{2\alpha}{2\alpha - 3} \right) K^{\frac{3}{\alpha}} \langle\sigma v\rangle^{\frac{3-\alpha}{\alpha}} (1 + z)^{\frac{9-4\alpha}{\alpha}} \\ &\quad \times \delta m (t - t_i)^{\frac{3-2\alpha}{\alpha}} m_\chi^{\frac{\alpha-3}{\alpha}}, \end{aligned} \quad (5)$$

where $K = (3 - \alpha)(4.66 \times 10^8)^{\alpha-3}(1 + z_{\text{eq}})^{\alpha/3}(4\pi)^{-1}$ cgs units, $n_\chi(r) = \rho_\chi(r)/m_\chi$ is the dark matter particle number density. The UCMH density profile can change from a steep slope $\alpha = 3$ (Mack et al. 2007) for the outer part region to $\alpha = 1.5$ (Bertschinger 1985) for the inner part region, if there is a PBH in the center of the UCMH. In particular, radial infall onto a central extended overdensity shows a profile

Notation and definition of some quantities in this paper

notation	definition	§/Eq.
$m_h(z)$	UCMH mass at redshift z	§2.1, eq. 1
$\rho_\chi(r, z)$	UCMH (density) profile at z	§2.1, eq. 2
$R_h(z)$	extent radius of UCMH	§2.1, eq. 3
m_χ	DM particle mass	§2.1, eq. 4
$\langle\sigma v\rangle$	DM average anni cross section	§2.1, eq. 4
L_{ann}	anni lum of a single UCMH	§2.1, eq. 5
f_{UCMH}	$f_{\text{UCMH}}(z_{\text{eq}}) = \Omega_{\text{UCMH}}(z_{\text{eq}})/\Omega_{\text{DM}}$	§2.1, eq. 7
l_{ann}	UCMH anni lum per volume	§2.1, eq. 10
l_{bkgd}	homogenous DM anni background	§2.1, eq. 11
l_{acc}	X-ray rad density from PBH host UCMHs	§2.2, eq. 13
f_{PBH}	$\Omega_{\text{PBH}}/\Omega_{\text{DM}}$	§2.2, eq. 13
r_B	Bondi accretion radius	§2.2, eq. 19
\mathcal{A}	amplification factor of the IGM T_m	§2.2, eq. 19
\dot{m}	Dimensional accretion rate	§2.2, eq. 23
f_b	baryonic fraction in a UCMH	§2.2, eq. 24
z_m	charac. redshift for gas accretion	§2.2, eq. 28
$x_{\text{ion}}(z)$	reionized baryon fraction at z	§3.1, eq. 35
$\epsilon(z)$	energy deposition rate per volume at z	§3.1, eq. 39
E_γ	photon energy from anni DM	§3.1, eq. 41
E_X	charac. energy for X-ray emission	§3.1, —
T_m	IGM gas temperature	§3.1, eq. 43
f_{H_2}	molecular hydrogen fraction in IGM gas	§3.1, eq. 47
L_{halo}	total anni lum from a dark halo	§4.1, —
L_{UCMH}	anni lum from UCMHs inside a halo	§4.1, —
L_{ext}	anni lum from extended DM in a halo	§4.1, —
$\epsilon_{\text{loc,iso}}$	energy deposited by isothermal DM halo anni	§4.1, eq. 48
$\epsilon_{\text{loc,UCMH}}$	energy deposited by UCMHs anni inside a halo	§4.1, eq. 49
$\epsilon_{\text{loc,acc}}$	energy deposited by X-rays inside a halo	§4.2, eq. 50
$z_m^{\text{halo}}/z_m^{\text{bkgd}}$	z_m for PBH host UCMHs inside/outside a halo	§4.2, —
$\epsilon_\delta(z)$	energy deposition rate density by δ -func SED	§5.3, eq. 52
factor	ratio of rad of differently distributed UCMHs	§5.4, eq. 64

Table 1. In this table “DM”, “anni”, “lum”, “charac.”, “rad”, “func” are short for dark matter, annihilation, luminosity, characteristic, radiation and function. The subscript “acc” is for X-ray emission because X-rays are emitted by gas accretion onto PBHs.

$\rho \propto r^{-9/4}$, which is more widely used as the typical density profile for most region in UCMHs (Ricotti & Gould 2009; Scott & Sivertsson 2009; Josan & Green 2010). Taking $\alpha = 9/4$, we have

$$L_{\text{ann}} = 36.3 L_\odot \langle\sigma v\rangle_s^{1/3} m_{\chi,100}^{-1/3} (1+z) \left(\frac{\delta m}{M_\odot} \right), \quad (6)$$

where $\langle\sigma v\rangle_s = \langle\sigma v\rangle/3 \times 10^{-26} \text{ cm}^3 \text{ s}^{-1}$ and $m_{\chi,100} = m_\chi c^2/100 \text{ GeV}$. According to equation (6), the annihilation luminosity decreases with the evolution of the Universe, basically because the annihilation flats the inner density profile as showed in equation (4). The left panel of Fig. 1 gives UCMH annihilation luminosity with different halo profile α and dark matter particle mass m_χ . Note that the annihilation luminosity can be much brighter for lighter dark matter particles, and a shallower density profile reduces L_{ann} significantly.¹ In the limit case $\alpha \simeq 1.5$ or 3, we have

¹ In Fig. 1 the annihilation luminosities following the density profile equation (2) are somewhat overestimated for a steep profile $\alpha \sim 3$, because in this case the halo mass within the truncated radius r_{cut} can no more be neglected. Thus the normalization factor of the density profile is $\propto [\ln(R_h/r_{\text{cut}})]^{-1}$, which is different from the factor $(3-\alpha)/(4\pi)$ in equation (2). However, as we show that L_{ann} for a steeper UCMH profile leads to several orders of magnitude higher L_{ann} than that with $\alpha = 2.25$, the conclusion that

$L_{\text{ann}} \propto \langle\sigma v\rangle/m_\chi$ or L_{ann} to be independent with m_χ and $\langle\sigma v\rangle$. The abundance of UCMH as the function of redshift is still uncertain today. It can be presented by a parameter

$$f_{\text{UCMH}}(z) = \Omega_{\text{UCMH}}(z)/\Omega_{\text{DM}}, \quad (7)$$

where Ω_{UCMH} and Ω_{DM} are the comoving abundances of UCMH and total dark matter with $\Omega_{\text{UCMH}}(z) = \Omega_{\text{UCMH}}(z_{\text{eq}})(1+z_{\text{eq}})/(1+z)$ and $\Omega_{\text{DM}}(z) = \Omega_{\text{DM}}(z=0)$. We have $f_{\text{UCMH}}(z=0) \sim f_{\text{UCMH}}(z_{\text{eq}})(1+z_{\text{eq}})/(1+10) \sim 3 \times 10^2 f_{\text{UCMH}}(z_{\text{eq}})$, which shows that the UCMH mass grows by up to two order of magnitude from z_{eq} to $z \sim 10$. From now on we take f_{UCMH} as $f_{\text{UCMH}}(z_{\text{eq}})$ for short to show the initial abundance of UCMH at matter-radiation equality, and in current stage f_{UCMH} is taken as a parameter for simplicity.

The mean free path of gamma-ray photons from an UCMH with energy E_γ is written as

$$\lambda_{\text{UCMH}} = \frac{1}{n_A(z)\sigma(E_\gamma)} \gg \frac{1}{n_A(z)\sigma_T} \approx 3 \times 10^3 \text{ pc} \left(\frac{1000}{1+z} \right)^3, \quad (8)$$

where $n_A(z) = n_A(1+z)^3$ is the atomic number density at redshift z . The average distance of inter-UCMH is estimated

a steeper profile gives a brighter annihilation will not be changed too much even in the limit case $\alpha = 3$. More details of the UCMH profile are discussed in Section 5.2.

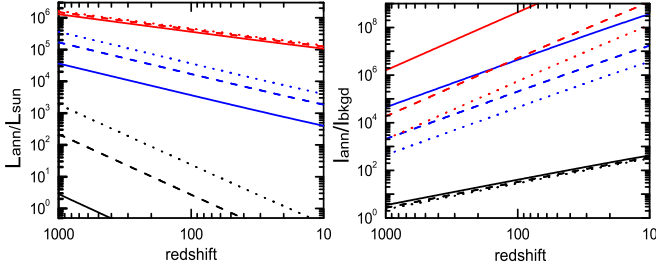


Figure 1. Left: UCMH dark matter annihilation luminosity with the halo profile $\alpha = 1.5$ (black lines), 2.25 (blue lines), 2.9 (red lines), and dark matter particle mass $m_\chi c^2 = 100$ GeV (solid lines), 1 GeV (dashed lines), 100 MeV (dotted lines). We adopt $\delta m = 1 M_\odot$ in this figure. Right: ratio of UCMH luminosity to homogenous dark matter background annihilation, where we take the fraction of UCMH in the total dark matter as $f_{\text{UCMH}} = 10^{-4}$ at $z = z_{\text{eq}}$, and the lines as the same as in left panel.

as

$$d_{\text{UCMH}} = \left[\frac{1}{n_{\text{UCMH}}(z)} \right]^{1/3} = \left[\frac{\langle \delta m \rangle}{f_{\text{UCMH}} \rho_{\text{DM}}(z)} \right]^{1/3} \sim 7 \text{ pc } f_{\text{UCMH},-4}^{-1/3} \left(\frac{\langle \delta m \rangle}{M_\odot} \right)^{1/3} \left(\frac{1000}{1+z} \right). \quad (9)$$

We have the mean free path exceed the inter-UCMH distance $\lambda_{\text{UCMH}} \gg d_{\text{UCMH}}$ except for an extremely small $f_{\text{UCMH}} \ll 10^{-12}$. Therefore the cosmic UCMH annihilation also gives an uniform gamma-ray background radiation field as well as that produced by the homogenous dark matter. UCMH annihilation luminosity per volume is given by

$$l_{\text{ann}} = \frac{L_{\text{ann}}}{\delta m} f_{\text{UCMH}}(z_{\text{eq}}) \rho_{\text{DM}}(z=0)(1+z)^3 = 1.4 \times 10^{-28} \text{ erg cm}^{-3} \text{ s}^{-1} \langle \sigma v \rangle_s^{1/3} m_{\chi,100}^{-1/3} f_{\text{UCMH}}(1+z)^4. \quad (10)$$

On the other hand, the energy injection rate by the self-annihilation of the homogenous dark matter background per volume is

$$l_{\text{bkgd}} = \langle \sigma v \rangle \frac{\rho_\chi^2 c^2}{2m_\chi} = 3.2 \times 10^{-43} \text{ erg cm}^{-3} \text{ s}^{-1} \langle \sigma v \rangle_s m_{\chi,100}^{-1} (1+z)^6. \quad (11)$$

We compare the radiation between UCMH and normal dark matter annihilation as

$$\frac{l_{\text{ann}}}{l_{\text{bkgd}}} = 4.5 \times 10^{12} \langle \sigma v \rangle_s^{-2/3} m_{\chi,100}^{2/3} \left(\frac{10}{1+z} \right)^2 f_{\text{UCMH}} \gg 1, \quad (12)$$

If $f_{\text{UCMH}} \geq 2.2 \times 10^{-15} \langle \sigma v \rangle_s^{2/3} m_{\chi,100}^{-2/3} (1+z)^2$, the gamma-ray background due to dark matter annihilation is dominated by UCMH annihilation. More details depending on the density profile α and dark matter m_χ can be seen in the right panel of Fig. 1.

2.2 Gas Accretion onto PBHs

The abundance of PBHs Ω_{PBH} as a fraction of total dark matter Ω_{DM} at $z < z_{\text{eq}}$ can be parameterized as $f_{\text{PBH}} = \Omega_{\text{PBH}}/\Omega_{\text{DM}}$. We ignore the PBH growth and take f_{PBH} as a constant in the matter-dominated Universe for two reasons. The first reason is that, as the accretion processes had been significantly suppressed before $z \sim 10$ due to the relative motion between PBHs and baryon gas, the PBH growth timescale is $t_{\text{growth}} \sim t_{\text{Salp}} \simeq 5 \times 10^8 \text{ yr}$ just reaches or is longer than the universe age at $t(z \sim 10) \sim 5 \times 10^8 \text{ yr}$. The second reason is that low mass PBHs has lower accretion rate while high mass PBHs are inclined to produce outflows, which further increases the accretion timescale and makes PBH growth to be negligible compared to its host UCMH growth. A very similar statement to keep a constant f_{PBH} was also proposed in Ricotti et al. (2008). Keep in mind the PBH abundance f_{PBH} is different from the UCMH initial abundance f_{UCMH} at z_{eq} as mentioned in Section 2.1, because a large amount of UCMH seeds at z_{eq} should be the initial primordial dark matter overdensity but not PBHs. According to the density primordial perturbation theory, generally we have the relation $f_{\text{PBH}} \ll f_{\text{UCMH}}$, which will be discussed in details in Section 2.2.1.

Much work has been done to show the effects of radiation from PBH or early black hole accretion on the early Universe thermal and ionization history (e.g., Barrow & Silk 1979; Gendin et al. 1995; Miller & Ostriker 2001; Ricotti 2007; Ricotti et al. 2008; Ripamonti et al. 2008). Our goal in this section is to focus on the importance of PBH gas accretion radiation compared to the overall UCMH dark matter annihilation. The X-ray emission from accreting PBHs may lead to a very different heating and ionization history of the early Universe compared to the dark matter annihilation. The X-ray luminosity from an individual PBH with mass M_{PBH} can be written as $\eta L_{\text{Edd}} = 4\pi\eta G m_p M_{\text{PBH}}/\sigma_T c \simeq 3.3 \times 10^3 \eta_{-1} L_\odot (M_{\text{PBH}}/M_\odot)$ with L_{Edd} and $\eta_{-1} = \eta/0.1$ being the Eddington luminosity and average radiation efficient of all PBHs respectively. This X-ray luminosity is much higher than the dark matter annihilation luminosity equation (6). Thus the X-ray radiation density in the early Universe $z > 10$ can be written as

$$l_{\text{acc}} = \left(\frac{L_{\text{Edd}}}{M_{\text{PBH}}} \right) \eta f_{\text{PBH}} \rho_{\text{DM}}(z=0)(1+z)^3 \simeq 1.3 \times 10^{-26} \text{ erg cm}^{-3} \text{ s}^{-1} \eta_{-1} f_{\text{PBH}} (1+z)^3. \quad (13)$$

Combining equations (10) and (13), the ratio between PBH accretion luminosity and UCMH dark matter annihilation luminosity is

$$\frac{l_{\text{acc}}}{l_{\text{ann}}} \simeq 9 \langle \sigma v \rangle_s^{-1/3} m_{\chi,100}^{1/3} \left(\frac{\eta_{-1} f_{\text{PBH}}}{f_{\text{UCMH}}} \right) \left(\frac{10}{1+z} \right). \quad (14)$$

Since the IGM heating rate due to the energy injection by PBH X-ray emission or UCMH dark matter annihilation is proportional to both the energy injection rate, and the IGM cross section for all the interactions suffered by the UCMH emitted photons in X-ray band E_X or annihilation emitted gamma-ray photons E_γ , the importance of the IGM gas heating by X-ray emission and UCMH dark matter annihilation can be estimated by the ratio $l_{\text{acc}} \sigma_{\text{tot}}(E_X)/l_{\text{ann}} \sigma_{\text{tot}}(E_\gamma)$ with σ_{tot} labeling the total cross sections in different photon energy range. If we roughly take the X-ray and IGM

interaction cross section $\sigma_{\text{tot}}(E_X)$ the Thomson cross section, and the high energy photon interaction $\sigma_{\text{tot}}(E_\gamma)$ the Klein-Nishina cross section (see Section 3.1 for more accurate calculations), the energy deposition in the IGM due to gas accretion ϵ_{acc} and annihilation ϵ_{ann} radiation is estimated as

$$\frac{\epsilon_{\text{acc}}}{\epsilon_{\text{ann}}} \simeq 3.2 \times 10^5 \langle \sigma v \rangle_s^{-1/3} m_{\chi,100}^{4/3} \left(\frac{\eta_{-1} f_{\text{PBH}}}{f_{\text{UCMH}}} \right) \left(\frac{10}{1+z} \right), \quad (15)$$

which gives the first conclusion that the X-ray heating may become totally dominated over dark matter annihilation in the early Universe if the PBH abundance exceeds a critical value as

$$\frac{\eta f_{\text{PBH}}}{f_{\text{UCMH}}} \geq 3.1 \times 10^{-7} \langle \sigma v \rangle_s^{1/3} m_{\chi,100}^{-4/3} \left(\frac{1+z}{10} \right). \quad (16)$$

Theoretically the value of $\eta f_{\text{PBH}}/f_{\text{UCMH}}$ includes many uncertainties. In general, there are at least three reasons to have a low value $\eta f_{\text{PBH}}/f_{\text{UCMH}} \ll 1$: density perturbation scenarios prefer low initially value of $f_{\text{PBH}}/f_{\text{UCMH}}$; inefficient radiation $\eta \ll 1$ is favored by low mass PBHs while accretion feedback decreases η for high mass PBHs or PBHs with high mass UCMHs; and X-ray emission from PBHs can be trapped inside the surrounding host UCMHs which accumulate baryons.

2.2.1 PBH Abundance

Either PBHs or UCMH overdensity seeds are produced basically by the density perturbation in the very early Universe during some special epochs such as inflation or phase transitions. The cosmological abundance of UCMHs can be estimated by integrating from the overdensity seed threshold $\sim 10^{-3}$, to the PBH formation threshold $\delta_c \sim 1/3$ (Ricotti & Gould 2009; Scott & Sivertsson 2009). Similarly, the PBH abundance is estimated by integrating the perturbation above $\delta_c \sim 1/3$ (Green & Liddle 1997; Green et al. 1997). Assuming a Gaussian perturbation at a formation redshift $z_f \gg z_{\text{eq}}$ to produce both PBHs and UCMH seeds, the ratio $f_{\text{PBH}}/f_{\text{UCMH}}$ at matter-radiation equality can be directly traced back to formation time z_f (Carr et al. 2010; Khlopov 2010). As a result, the relative abundance of PBHs to UCMH overdensity seeds formed at redshift z_f is written as

$$\begin{aligned} \frac{f_{\text{PBH}}}{f_{\text{UCMH}}} &= \frac{\int_{\delta_c}^1 \exp \left[-\frac{\delta^2}{2\sigma(z_f)^2} \right] d\delta}{\int_{10^{-3}}^{\delta_c} \exp \left[-\frac{\delta^2}{2\sigma(z_f)^2} \right] d\delta} \\ &\simeq \exp \left[\frac{10^{-6} - \delta_c^2}{2\sigma^2} \right] \simeq \exp \left(-\frac{1}{18\sigma^2} \right). \end{aligned} \quad (17)$$

The perturbation variance at z_f is roughly given by $\sigma(z_f) \simeq 9.5 \times 10^{-5} [M_{\text{hor}}(z_f)/10^{56} \text{ g}]^{(1-n)/4}$ (Green & Liddle 1997), with $M_{\text{hor}}(z_f)$ and n being the horizon mass and mass spectrum index at z_f . Taking $n \leq 1.3$ (Lidsey et al. 1995), the ratio $f_{\text{PBH}}/f_{\text{UCMH}}$ from a Gaussian perturbation is the function of horizon mass as

$$\frac{f_{\text{PBH}}}{f_{\text{UCMH}}} \leq \exp \left[-\left(\frac{M_{\text{hor}}(z_f)}{5.5 \times 10^{10} \text{ g}} \right)^{(n-1)/2} \right], \quad (18)$$

which means the value of $f_{\text{PBH}}/f_{\text{UCMH}}$ becomes $\ll 1$ for $M_{\text{hor}}(z_f) \gg 5.5 \times 10^{10} \text{ g}$, not to mention the fact that

the masses of dark matter overdensity seeds or PBHs are even lower than the horizon mass $\delta m \ll M_{\text{hor}}(z_f)$ and $M_{\text{PBH}} \ll M_{\text{hor}}(z_f)$. Combining equations (15) and (18), X-ray emission from gas accretion hardly becomes the dominated heating source in the early Universe, except for low mass PBHs $M_{\text{PBH}} \ll M_{\text{hor}}(z_f) < 3.7 \times 10^{18} \text{ g}$ in the Gaussian perturbation scenario. However, PBHs in this mass range should either have disappeared within a Hubble time due to the Hawking evaporation, or too small to accrete the IGM gas.

As a result, the initially Gaussian density perturbation at a certain epoch is not able to generate sufficient abundant PBH to dominated over the total UCMH dark matter annihilation emission, basically because the large amplitude part of a Gaussian distribution is highly suppressed. On the other hand, non-Gaussian perturbation may give an even lower probability of PBH formation, as the large fluctuation can be suppressed in the non-Gaussian distribution and further decrease the ratio of $f_{\text{PBH}}/f_{\text{UCMH}}$ (Bullock & Primack 1997).

However, other mechanisms such as different formation epochs for UCMHs and PBHs, different early inflationary potential, double inflation models, various phase transitions, and cosmic string collapse may enhance the high amplitude perturbation and increase the PBH abundance (see Khlopov 2010 and references therein). Also, it is still arguable if all the $\delta > 10^{-3}$ perturbation could produce dark matter overdensity in the radiation dominant era. For example, Ricotti & Gould (2009) requires the host UCMHs around PBHs to have similar initial perturbation amplitude as PBHs, while Scott & Sivertsson (2009) has less strict requirement as $\delta > 10^{-3}$ to form the initial dark matter overdensity. There are more physical uncertainties to estimate the abundance of PBHs and UCMHs produced by other mechanisms than a simple Gaussian distribution assumption. Therefore we still take f_{PBH} as a free parameter which satisfies $f_{\text{PBH}} \ll f_{\text{UCMH}}$ to describe the relative abundances between PBHs and UCMHs.

2.2.2 Inefficient Radiation

Another effect to constrain the X-ray luminosity density in the early Universe by the gas accretion onto PBHs is the low radiation efficiency due to low accretion rate onto low mass PBHs, or the significant radiative feedback, thermal outflow and suppressed accretion rate due to accretion onto high mass PBHs or PBHs with high mass host UCMHs.

In principle the mass distribution of PBHs is broad enough to cover the range from the Planck mass $\sim 10^{-5} \text{ g}$ to thousands of solar mass $10^5 M_\odot$ (e.g., Carr et al. 2010). As mentioned in the above Section 2.2.1, if PBHs are formed from the Gaussian perturbation with the variation $\sigma \propto M^{-(n-1)/4}$ and the index $n > 1$, low mass PBHs should be more abundant because of the higher density perturbation variance σ for lower mass M . Also, phase transition models give PBH mass or UCMH seed less than $1 M_\odot$ (Scott & Sivertsson 2009). On the other hand, keep in mind in the IGM environment a “naked” PBH without a host UCMH can never reach the Eddington accretion rate $\dot{M}_{\text{Edd}}^{\text{PBH}} = L_{\text{Edd}}/c^2 \simeq 1.4 \times 10^{17} (M_{\text{PBH}}/M_\odot) \text{ g s}^{-1}$, unless its mass is $M_{\text{PBH}} \geq 360 M_\odot [1000/(1+z)]^{3/2}$. The surrounding host UCMH increases the accretion rate if the PBH mass

is $M_{\text{PBH}} > 100M_{\odot}$ (Ricotti et al. 2008, their Fig. 4). Note that an ideal case is $\eta \simeq \min\{0.1\dot{m}, 1\}$ after the accretion become super-Eddington, while the typical accretion efficiency for quasars or microquasars disk is $\eta \sim 0.15$. For low mass PBHs with $\dot{m} \ll 1$ the radiation efficiency is estimated as $\eta \simeq 0.01\dot{m}^2$ for the spherical case (Shapiro 1973a,b), which gives much lower efficiency than the high accretion rate that $\eta \ll 0.1$.

If high mass PBHs ($100M_{\odot} < M_{\text{PBH}} < 10^5M_{\odot}$) successfully form with an appreciable abundance compared to the low mass PBHs, as discussed by some previous authors (Mack et al. 2007; Saito et al. 2008; Frampton et al. 2010), or the host UCMH seeds are more massive than the PBHs $\delta m \gg M_{\text{PBH}}$ (Ricotti & Gould 2009, more details see Section 2.2.3), the Bondi accretion rates onto these PBHs with their host UCMHs can significant exceed the Eddington limit after some critic redshifts (Ricotti et al. 2008). However, a spherical super-Eddington accretion is generally unstable and inclined to drive high mass loss rate with thermal outflows (e.g., Smith & Owocki 2006). Recent simulations show that radiative feedback may become important to reduce or even quench the accretion process periodically (Milosavljević et al. 2009a,b; Park & Ricotti 2011). Also, the thermal heating by the outflow energy or radiative feedback will increase the temperature of the gas around PBHs and decrease the Bondi radius and accretion rate onto PBHs. Besides the spherical accretion case, the falling gas angular momentum will become important for $\dot{m} \gg 1$, and form an accretion disk around PBHs. However, the physics of the super-Eddington accretion disks is still not clearly known. Various types of super-Eddington accretion disk models have been proposed, such as the optically-thick advection dominated accretion flow (ADAF, Narayan & Yi 1994, Narayan et al. 1998), the adiabatic inflow-outflow (ADIO, Blandford & Begelman 1999), the convection-dominated accretion flow (CDAF, Narayan et al. 2000), the “polish doughnuts” torus (Abramowicz et al. 1978) and the thick slim disk (Abramowicz et al. 1988). In most cases the super-Eddington accretion disk advects most of its heating energy inward into the black hole without emission, and has a low radiation efficiency η for high accretion rate $\eta < 1$ (Abramowicz et al. 1988; Narayan et al. 1998 or Abramowicz & Fragile 2011 for a review).

In a brief summary, low average radiation efficiency η in equations (13) to (15) are favored because of the low accretion rate onto the low mass PBHs, and radiative or viscous feedback and outflows of accretion onto high mass PBHs or PBHs with high mass host UCMHs, which also leads to a low value of $\eta f_{\text{PBH}}/f_{\text{UCMH}}$ and suppress the importance of PBH X-ray radiation from PBHs compared to the overall UCMH dark matter annihilation. From now on we consider the X-ray emission is mainly contributed by the accreting PBHs with $\dot{m} \gg 1$.

2.2.3 Radiation Trapping in Host UCMHs

Some previous works discussed that the accretion flow around PBHs is Compton thin in most cases, since in the sub-Eddington accretion case the spherical flow is transparent near the PBH, while in the super-Eddington accretion case the accretion flow are inclined to form an accretion

disk (e.g., Ricotti et al. 2008). However, sufficient high mass UCMHs can accrete and thermalize baryons from the ambient IGM, *even there are no PBHs in the center of these UCMHs*. As the gravity potential at the outer edge of the host UCMH is mainly contributed by the UCMH mass, but the accretion onto the center PBHs is according to the PBH mass, the accretion rate into the host UCMHs is not necessarily equal to the accretion rate onto the center PBHs. In other words, baryons can be firstly accumulated and virialized inside the host UCMH during the accretion from the IGM to the inner UCMH region, followed by a secondary accretion onto the center PBH and feedback (outflow) from the accreting PBHs. Based on this consideration, the baryons inside the UCMH can be divided into two components: the piled up baryons inside the UCMH, and the accretion spherical flow or disk around the center PBH. Although the optical depth of the accretion gas or disk, which is mainly contributed by the depth around the inner horizon region $r \sim R_{\text{Sch}}$ is transparent to X-ray photons, the X-ray emission can still be trapped and absorbed by the piled up baryons inside the host UCMH, and reradiate photons with much longer wavelength into the outer IGM environment. Quantitative analysis is given as follows. Part of the treatment is similar to an analogy discussion on the dark matter structure formation and baryons filling process (Hoeft et al. 2006; Okamoto et al. 2008).

If UCMH dark matter annihilation does not change the IGM temperature evolution, the IGM temperature is approximately coupled with the cosmic microwave background (CMB) temperature before the decoupling time $z_{\text{dec}} \sim 100$, and the IGM sound speed before z_{dec} is $c_s \simeq 5.7 \text{ km s}^{-1} \left(\frac{1+z}{1000}\right)^{1/2}$. In general, the UCMH annihilation heating and PBH emission without trapping increases the IGM temperature. We introduce an amplification factor \mathcal{A} that $T_{\text{m}} = \mathcal{A}T_{\text{CMB}}$ at $z > z_{\text{dec}}$, where T_{m} and T_{CMB} are the temperature of the IGM and CMB respectively, and \mathcal{A} depends on the UCMH profile and annihilation properties, as we will calculate in Section 3. The sound speed $c_s \propto T^{1/2}$ becomes $c_s \simeq 5.7 \text{ km s}^{-1} \mathcal{A}^{1/2} \left(\frac{1+z}{1000}\right)^{1/2}$, and the Bondi accretion radius (i.e., the accretion sonic sphere) of a PBH-UCMH system at $z > z_{\text{dec}}$ is

$$r_B \approx \frac{Gm_h}{c_s^2} \approx \frac{400 \text{ pc}}{(1+z)^2} \mathcal{A}^{-1} \left(\frac{\delta m}{M_{\odot}} \right). \quad (19)$$

Equation (19) is derived under the assumption that the Bondi radius is larger than the UCMH size $r_B > R_h$. Furthermore, if $r_B > 2R_h$, the virial temperature of the host UCMH $T_{\text{vir}} \simeq \left(\frac{\mu m_p}{2k_B}\right) \left[\frac{Gm_h(z)}{R_h}\right]$ is greater than the temperature of the ambient IGM gas $T_{\text{vir}} > T_{\text{m}}$. According to the general virial theorem, the thermal pressure of the gas due to virialized heating is weak compared to gravity of the UCMH. In this case we consider the IGM baryons should fall into the UCMH unimpeded, regardless of the center PBH mass (Hoeft et al. 2006; Okamoto et al. 2008).

The criterion $r_B > 2R_h$ at $z > z_{\text{dec}}$ gives

$$\left(\frac{\delta m}{M_{\odot}} \right) > 1600 \mathcal{A}^{3/2} \left(\frac{1+z}{1000} \right). \quad (20)$$

Note that higher IGM temperature around UCMH, i.e., higher \mathcal{A} gives a higher minimum UCMH mass to attract baryons. Similar result can be derived for the case after de-

coupling $z < z_{\text{dec}}$, where the IGM gas temperature decoupled with the CMB temperature and dropped adiabatically as $T_{\text{ad}} \propto (1+z)^2$ without any heating sources. We still take the factor $\mathcal{A} \geq 1$ to measure the IGM temperature increase due to annihilation $T_{\text{m}} = \mathcal{A}T_{\text{ad}}$. Then using the criterion $r_B > 2R_h$, we find that baryons fall into UCMHs unimpeded at $z < z_{\text{dec}}$ if

$$\left(\frac{\delta m}{M_{\odot}}\right) > 160\mathcal{A}^{3/2} \left(\frac{1+z}{100}\right)^{5/2}. \quad (21)$$

As a result, if the UCMH initial overdensity seed is $\delta m > 1600\mathcal{A}^{3/2}M_{\odot}$ for $z_{\text{dec}} < z < 1000$, or $\delta m > 160\mathcal{A}^{3/2}M_{\odot}$ for $z < z_{\text{dec}}$, the IGM gas can always fill into the UCMH *no matter it includes a PBH or not*. Otherwise for a lower δm , the critical redshift z_c below which the UCMH accrete is $(1+z_c) < 0.63\mathcal{A}^{-3/2}(\delta m/M_{\odot})$ for $z > z_{\text{dec}}$ and $(1+z_c) < 13\mathcal{A}^{-3/5}(\delta m/M_{\odot})^{2/5}$ for $z < z_{\text{dec}}$. If the UCMH hosts a PBH in the center, baryons are still able to pile up and thermalized in the host UCMH due to the gas virialization.

The lower bound of gas accretion rate into the UCMH can be estimated as

$$\begin{aligned} \dot{M}_{\text{UCMH}} &= 4\pi r_B^2 c_s \rho_{\text{gas}}(z) > 4\pi R_h^2 v_{ff}(R_h) m_b n_b(z) \\ &\sim 8.2 \times 10^{16} \text{ g cm}^{-3} (1+z)^{1/2} \left(\frac{\delta m}{M_{\odot}}\right), \end{aligned} \quad (22)$$

where $v_{ff}(R_h)$ is the free fall velocity at R_h . If all the gas into the UCMH is totally accreted onto the center PBH, the dimensionless accretion rate of the PBH is $\dot{m} = \dot{M}_g/\dot{M}_{\text{Edd}}^{\text{PBH}}$ is

$$\dot{m} > 18.0 \left(\frac{1+z}{1000}\right)^{1/2} \left(\frac{\delta m}{M_{\text{PBH}}}\right) > 1, \quad (23)$$

with $\dot{M}_{\text{Edd}}^{\text{PBH}}$ being the Eddington limit accretion rate onto the central PBH. Note that the ideal \dot{m} can be even higher if the initial host UCMH is more massive than the center PBH $\delta m \gg M_{\text{PBH}}$ as discussed in Ricotti & Gould (2009). However, the real accretion rate should be less than the value in equation (23) for two reasons. First, the baryons can be heated and virialized during the accretion process in the UCMH, and has a temperature $\sim T_{\text{vir}}$ warmer than the IGM T_{m} to increase the gas pressure and decrease the accretion rate onto the PBH. And the gas temperature is further increased $\gg T_{\text{vir}}$ near the PBH due to PBH emission and ionization. Also, super-Eddington accretion disks are also inclined to drive outflows. The positive Bernoulli parameter over most of the ADAFs due to the small radiation loss may trigger strong outflows or jets (Narayan & Yi 1994), and produce an ADIOs in which outflow carries away most of flow mass and energy (Blandford & Begelman 1999). Also, CDAFs may produce a “convective envelope” with no accretion onto the black hole (Narayan et al. 2000). In general accretion disks with super-Eddington accretion rate are inevitably accompanied by outflows and winds, which significantly decrease the final accretion rate onto the black hole. In the PBH case, these outflows should be injected back to the host UCMH environment.

The upper bound of the baryonic fraction in the UCMH is the universal fraction Ω_b/Ω_m . However, as the UCMH grows following equation (1), we adopt a more conservative method to estimate the lower bound of baryon fraction f_b inside the UCMH. We estimate the baryonic fraction in the UCMH f_b (the mass ratio between gas and dark matter) as

$$(\dot{M}_{\text{UCMH}} - \dot{M}_{\text{PBH}})(t - t_i) \sim m_h(z) f_b \quad (24)$$

where we take $\dot{M}_{\text{UCMH}} \gg \dot{M}_{\text{PBH}}$, i.e., most of the accreted gas into the UCMH is piled up without being immediately eaten by the PBH. Combining equations (22) and (24), we have the lower bound of baryon fraction to be $f_b \geq 7.6 \times 10^{-3}$, which is a constant independent of the redshift.

The optical depth of the piled up gas in the UCMH due to Compton scattering is

$$\tau \sim x_e \sigma_T \int \frac{\rho_{\chi}(r) f_b}{\mu m_p} dr. \quad (25)$$

Since f_b from equation (24) is a constant, and UCMH growth does not change the steep region $\rho_{\text{DM}} \propto r^{-\alpha}$ with $\alpha = 9/4$ but only increase R_h and flats the region $r < r_{\text{cut}}$ (see equation [4]), we take the baryon fraction to be uniformly distributed in the UCMH, both in the steep and flat region. Therefore the column density of the baryon gas inside the UCMH depends on the UCMH profile, which depends on the dark matter properties ($\langle \sigma v \rangle, m_{\chi}$) given by equation (4). Actually the baryon profile can be steeper in the flat region of the halo $r < r_{\text{cut}}$ since the dark matter annihilation flats the inner halo profile, thus gives an even larger optical depth. Furthermore, we consider the baryon gas is ionized $x_e \sim 1$ inside the UCMH, at least in the flat region $r < r_{\text{cut}}$. We check that the Strömgren radius of the PBH emission r_S satisfies $r_{\text{cut}} < r_S < R_h$, as the heated gas near the PBH can reach a temperature as high as the Compton temperature ~ 10 keV in the ionized region. The hot ionized gas around the PBH produces a small sonic sphere in the dense baryon region near the PBH, decreases the accretion rate onto the PBH, giving $\dot{M}_{\text{UCMH}} \gg \dot{M}_{\text{PBH}}$ as mentioned in equation (24). Note that there should be two distinct sonic spheres, the sphere for the host UCMH outside R_h , and that for the center PBH inside the UCMH. This scenario is similar with Wang et al. (2006) that an accreting BH has two Bondi spheres, a smaller inner sphere in the hot gas region and a larger one in the outer cooler region. Therefore we take $x_e \sim 1$ in equation (25). The optical depth is written as

$$\begin{aligned} \tau &\sim \left(\frac{\sigma_T f_b}{\mu m_p}\right) \int \rho_{\chi}(r) dr \\ &\geq 10 \left(\frac{\delta m}{M_{\odot}}\right)^{1/3} \left(\frac{1+z}{1000}\right)^{5/6} m_{\chi,100}^{5/9} \langle \sigma v \rangle_s^{-13/9}, \end{aligned} \quad (26)$$

Hereafter we take $\langle \sigma v \rangle_s = 1$. Combining equations (20) and (26), we conclude that before the decoupling $z > z_{\text{dec}}$ the gas is always Compton thick to the X-ray emission from the center PBH accretion when the host UCMH itself accretes baryons. After the decoupling $z < z_{\text{dec}}$ the redshift range that X-ray emission escapes is

$$\begin{cases} (1+z) < 13 \left(\frac{\delta m}{M_{\odot}}\right)^{2/5} \mathcal{A}^{-3/5} & \left(\frac{\delta m}{M_{\odot}}\right) < 7m_{\chi,100}^{-5/6} \mathcal{A}^{3/4} \\ (1+z) < 62 \left(\frac{\delta m}{M_{\odot}}\right)^{-2/5} m_{\chi,100}^{-2/3} & \left(\frac{\delta m}{M_{\odot}}\right) > 7m_{\chi,100}^{-5/6} \mathcal{A}^{3/4} \end{cases} \quad (27)$$

From equation (27) there is a maximum z_m in the case of $r_B > 2R_h$ that

$$z_m^{(r_B > 2R_h)} = 29m_{\chi,100}^{-1/3} \mathcal{A}^{-3/10} - 1, \quad (28)$$

if $z > z_m$, X-ray photons will be totally trapped. Note that z_m insensitively decreases with the increasing of the IGM temperature factor \mathcal{A} . A larger optical depth due to a deeper

baryon profile at $r < r_{\text{cut}}$ gives an even lower z_m . Also, the range of δm applied in equation (27) is

$$0.64M_{\odot}\mathcal{A}^{3/2} < \delta m < 80M_{\odot}m_{\chi,100}^{-5/3}. \quad (29)$$

In other words, in the $r_B > 2R_h$ case, no X-rays can escape the host UCMH if $\delta m \geq 80M_{\odot}m_{\chi,100}^{-5/3}$. More massive PBHs are easier to reach Eddington accretion rate, but more difficult to produce a transparent baryon environment in the host UCMHs.

On the other hand, if $r_B < 2R_h$ (i.e., $T_{\text{vir}}(R_h) < T_m$), most part of the UCMH gravity potential well is not deep enough to compress the gas and overcome the pressure barrier of the gas virialization heating. In this case the UCMH itself cannot accrete and thermalize baryons except for the region in the radius r'_B where satisfies $[Gm_h(r \leq r'_B)/(2r'_B)] = c_s^2$. At $z > z_{\text{dec}}$, the critical radius r'_B for a pure UCMH profile $\rho_{\chi} \propto r^{-\alpha}$ is

$$r'_B = R_h \left(\frac{Gm_h}{2c_s^2 R_h} \right)^{1/(\alpha-2)}, \quad (30)$$

where we apply $\alpha = 9/4$ from equation (5). The part of UCMH inside r'_B can accrete and heat baryons. Similar to equations (22) to (26), the accretion rate into the region $r \leq r'_B$ in the unit of Eddington accretion rate of the center PBH at $z > z_{\text{dec}}$ is

$$\begin{aligned} \dot{m} &= \frac{2\pi r_B'^2 c_s m_b n_b(z)}{\dot{M}_{\text{Edd}}^{\text{PBH}}} \\ &\approx 3.9 \times 10^{-11} \mathcal{A}^{-15/2} \left(\frac{100}{1+z} \right)^{9/2} \left(\frac{\delta m}{M_{\odot}} \right)^5 \left(\frac{\delta m}{M_{\text{PBH}}} \right)^{-3}, \end{aligned} \quad (31)$$

where the factor 2π is due to the suppressed accretion at $r > r'_B$ in the UCMH, thus the baryon density is half of the ambient gas density. Assuming $\delta m = M_{\text{PBH}}$, equation (31) shows that only high mass PBHs ($M_{\text{PBH}} > 100M_{\odot}$) are able to produce super-Eddington accretion if there is no accretion feedback. This is basically consistent with the results in Ricotti et al. (2008). However, we should mention two things. The first thing is that, if $\delta m > M_{\text{PBH}}$, the ideal accretion rate in equation (31) also increases. The second thing, which is similar to the analysis below equation (23) is that, the real accretion rate onto the PBH is lower than the ideal \dot{m} due to higher gas temperature and accretion feedback. As a result, we find that baryons can be accumulated and virialized inside the UCMH region $r \leq r'_B$ with a baryon fraction approximately as $f_b \sim 10^{-3} \mathcal{A}^{-9/2} (1+z)^{-3} (\delta m/M_{\odot})^3$. Using the condition $\dot{m} > 1$ in equation (31) at $z > z_{\text{dec}}$ for a sufficient radiation efficiency, the baryon optical depth inside radius r'_B is

$$\begin{aligned} \tau &\sim 1.1 \times 10^{-2} \mathcal{A}^{-9/2} (1+z)^{-13/6} m_{\chi,100}^{5/9} \left(\frac{\delta m}{M_{\odot}} \right)^{10/3} \\ &> 5.0 m_{\chi,100}^{5/9} \mathcal{A}^{1/2} \left(\frac{M_{\text{PBH}}}{\delta m} \right)^{2/3} \left(\frac{1+z}{100} \right)^{5/6} > 1, \end{aligned} \quad (32)$$

where we also take the baryon profile inside the UCMH is proportional to the dark matter profile for simplicity, and $x_e \sim 1$. According to equation (32), we consider the UCMH is optically thick to the X-ray emission in the case of $r_B < 2R_h$ and $z > z_{\text{dec}}$, unless $\delta m \gg M_{\text{PBH}}$ or dark matter particle mass $m_{\chi,100} \ll 1$.

After decoupling $z < z_{\text{dec}}$, we find that baryons can be accumulated and virialized inside a radius

$$r'_B \approx 0.012 \text{ pc } \mathcal{A}^{-4} \left(\frac{30}{1+z} \right)^8 \left(\frac{\delta m}{M_{\odot}} \right)^3 \quad (33)$$

with an upper bound z_m that

$$z_m^{(r'_B < 2R_h)} \simeq 32 \mathcal{A}^{-3/8} \left(\frac{\delta m}{M_{\text{PBH}}} \right)^{1/2} m_{\chi,100}^{-5/12} - 1, \quad (34)$$

below which ($z < z_m$) the gas is Compton thin inside radius r'_B . Higher ratio $\delta m/M_{\text{PBH}} \gg 1$ or lighter dark matter $m_{\chi,100} \ll 1$ increases z_m , which also decreases slightly if annihilation effect is included to heat the IGM gas ($\mathcal{A} > 1$).

Not only the baryons inside UCMHs can trap X-ray photons, but also the outflows driven by PBH accretion feedback also absorb the X-ray emission as well. As mentioned before, the super-Eddington accretion rate onto the PBH is unstable to trigger strong outflows in both spherical and disk cases. An optically thick “outflow envelope”, both in the polar and equatorial region around the PBHs, forms to cover the PBH and totally or mostly absorb X-ray emission from the inner accretion flows (Igumenshchev et al. 2003; Kohri et al. 2005; Poutanen et al. 2007; Abolmasov et al. 2009). In this case, the Compton heating in the outflow region should be important to increase the gas pressure and temperature, balance the gravity well, reemit thermalized photons from outflows, and regular and the accretion rate onto the PBH (Wang et al. 2006). It is likely to have a steady state or periodically changing outflow envelope covering the whole PBH, but the details are still an open question which is beyond the purpose of this paper. What we want to show is that, even though the accretion disk itself around PBH is optical thin to X-ray radiation, the X-ray emission can be still absorbed in the outflow envelope due to the accretion feedback and disk instability in the super-Eddington case, not to mention the optical-thick or geometry thick disks which absorb X-ray emission by themselves.

We give a summary of Section 2.2. Equation (13) computes the X-ray radiation density due to baryon gas accretion onto PBHs. The ratio $\eta f_{\text{PBH}}/f_{\text{UCMH}}$ is parameterized in this paper. The much lower probability of PBH formation compared to the UCMH formation, and inefficient radiation due to low mass PBHs ($\delta m \ll 100M_{\odot}$) or accretion feedback from high mass PBHs or PBHs with massive UCMHs ($\delta m \gg M_{\text{PBH}}$) give $\eta f_{\text{PBH}}/f_{\text{UCMH}} \ll 1$. Moreover, we simply introduce a critical redshift z_m below which ($z < z_m$) X-ray emission from the super-Eddington accretion PBHs ($\dot{m} \gg 1$) become important to heat and ionize the early Universe. Hotter IGM heated by other energy sources (e.g., annihilation) slightly decreases z_m . Ricotti et al. (2008) showed that the accretion becomes $\dot{m} \gg 1$ at $z_m \sim 20$ (100) for $M_{\text{PBH}} = 10^2$ (300) M_{\odot} , and \dot{m} is always $\dot{m} \gg 1$ ($\dot{m} \ll 1$) for $M_{\text{PBH}} > 10^3 M_{\odot}$ ($M_{\text{PBH}} \ll 10 M_{\odot}$). However, as we discussed in Section 2.2.3, the stage of super-Eddington accretion heating the IGM can be delayed, because X-ray photons are trapped inside the total or inner region of the UCMHs due to the accumulation and virialization of the accretion gas. Outflows can also (partly) absorb X-rays. We take the critical redshift z_m as showed in equations (28) and (34), for $z < z_m$ X-ray photons from the super-Eddington accretion PBHs could escape their host UCMHs. If the PBH abundance is much less than that of UCMH, but still satisfies equation (16), X-ray emission should dominate over the early dark matter annihilation at $z < z_m$.

3 REIONIZATION AND HEATING OF THE IGM

3.1 Basic Equations

The evolution of baryon ionization fraction $x_{\text{ion}}(z)$ is given by the differential equation (e.g., Cirelli et al. 2009)

$$n_A(1+z)^3 \frac{dx_{\text{ion}}(z)}{dt} = I(z) - R(z), \quad (35)$$

where $I(z)$ and $R(z)$ are the ionization and recombination rates per volume respectively, n_A is the atomic number density today. We use the rate $R(z)$ from Natarajan & Schwarz (2008). The ionization rate per volume due to dark matter annihilation or X-ray emission from gas accretion is given by

$$I(z) = \int_{E_{\text{eq}}}^{E_X} dE_\gamma \frac{dn(z)}{dE_\gamma} P(E_\gamma, z) N_{\text{ion}}(E_\gamma), \quad (36)$$

where $E_X = m_\chi c^2$ is the maximum energy of the emitted photon, $E_{\text{eq}} \simeq E_X(1+z)/(1+z_{\text{eq}})$, the differential term $dn(z)/dE_\gamma$ is the photon spectral number density at redshift z . We follow Cirelli et al. 2009 (see also Belikov & Hooper 2009; Natarajan & Schwarz 2008, 2009) to calculate the probability of primary ionizations per second $P(E_\gamma, z)$, and the number of final ionizations that generated by a single photon of energy E_γ produces $N_{\text{ion}}(E_\gamma)$. Note that $N_{\text{ion}}(E_\gamma)$ is proportional to the ionization factor $\eta_{\text{ion}}(x_{\text{ion}}) \approx (1 - x_{\text{ion}})/3$ (Shull & van Steenberg 1985; Chen & Kamionkowski 2004), which means approximately 1/3 emitted energy goes into the reionization of atoms if $x_{\text{ion}} \ll 1$.

First of all, we consider the ionization is due to UCMH dark matter annihilation. The spectral number density is obtained as

$$\frac{dl_{\text{ann}}(z)}{dE_\gamma} = \int_0^z dz' \frac{cdt}{dz'} \frac{dl_{\text{ann}}(z')}{E_\chi dE_{\gamma'}(z')} \left(\frac{1+z}{1+z'} \right)^3 \exp(-\tau), \quad (37)$$

where l_{ann} is the annihilation luminosity as mentioned in Section 2.1. $E_{\gamma'}(z') = E_\gamma(1+z')/(1+z)$. The optical depth τ is

$$\tau = \int_{z'}^z dz'' \frac{cdt}{dz''} n_A(1+z'')^3 \sigma_{\text{tot}}(E_{\gamma''}) \quad (38)$$

with $E_{\gamma''} = E_{\gamma'}(1+z'')/(1+z')$. The total cross section σ_{tot} for the DM annihilation photon to interact with electrons in the IGM mainly includes the Klein-Nishina cross section for Compton scattering (Rybicki & Lightman 2004) and the photoionization cross section for H and He as $\sigma_{\text{H+He}}$ (Zdziarski & Svensson 1989). Pair production on matter becomes important for $m_\chi > 1$ GeV. CMB photons also contribute to the total cross section for $m_\chi > 10$ TeV, which can be neglected in our cases.

The total energy deposition per second per volume at redshift z is given by

$$\epsilon(z) = \int_{E_{\text{eq}}}^{E_X} dE_\gamma \frac{dn_{\text{ann}}(z)}{dE_\gamma} n_A(1+z)^3 \sigma_{\text{tot}}(E_\gamma) E_\gamma. \quad (39)$$

If we take the monochromatic dark matter annihilation emission for simplicity, i.e., the photons produced by dark matter annihilation are the rest energy of the dark matter particle $m_\chi c^2$, the photon flux spectral density then can be calculated by the δ -function

$$\frac{dl_{\text{ann}}}{dE_{\gamma'}}(z') \approx l_{\text{ann}}(z') \delta(E_{\gamma'} - E_X). \quad (40)$$

Thus we have the energy deposition $\epsilon(z)$ as

$$\epsilon(z) = \int_{E_{\text{eq}}}^{E_X} \frac{dE_\gamma}{E_X} n_A(1+z)^4 \frac{cdt}{dz'_0} l_{\text{ann}}(z'_0) \left(\frac{1+z}{1+z'_0} \right)^3 e^{-\tau} \sigma_{\text{tot}}(E_\gamma), \quad (41)$$

where z'_0 satisfies

$$z'_0 = \frac{E_X}{E_\gamma}(1+z) - 1, \quad (42)$$

and τ is calculated from z'_0 to z . Keep in mind in the above formula (41) the dark matter annihilation products are simplified as the gamma-ray photons with sole energy $E_X = m_\chi c^2$. More realistic annihilation spectrum is model-dependent. For example, dn/dE_γ can be chosen as following the model in Bergström et al. (1998) and Feng et al. (2001).

For the X-ray photons from an accreting PBH, equation (41) will still be available if we choose σ_{tot} as the X-ray total cross section $\sigma_{\text{tot}} \approx \sigma_{\text{H+He}} + \sigma_T$, and E_X with the X-ray characteristic energy E_X as $E_X \simeq 3$ keV $(M_{\text{PBH}}/M_\odot)^{-1/4}$ (Salvaterra et al. 2005). As the real accreting PBH spectral energy distribution is very model-dependent (e.g., Shakura & Sunyaev 1973; Sazonov et al. 2004; Salvaterra et al. 2005; Ripamonti et al. 2008), in the very first calculation we simplify the X-ray emission as the single-frequency emission at a characteristic energy E_X , which mostly can be considered as the peaked energy in the real spectral energy distribution. We will also discuss the more realistic PBH spectral energy distribution in the discussion section 5.3.

Now we list the heating and cooling processes in the IGM. The heating of IGM by UCMH annihilation or X-ray emission can be written as

$$\left(\frac{dT_m}{dt} \right)_{\text{ann}} = \frac{2}{3k_B} \frac{\eta_{\text{heat}}(x_{\text{ion}})}{n_A(1+z)^3(1+f_{\text{He}}+x_{\text{ion}})} \epsilon(z), \quad (43)$$

where the heating fraction $\eta_{\text{heat}}(x_{\text{ion}})$ which shows the portion of energy $\epsilon(z)$ into heating IGM is adopted as $\eta_{\text{heat}} = C(1 - (1 - x_{\text{ion}}^a))^b$ with $C = 0.9971$, $a = 0.2663$ and $b = 1.3163$ (Shull & van Steenberg 1985). We can approximate take the He fraction in the IGM as $f_{\text{He}} \simeq 0.073$. Moreover, CMB photons can be treated as another heating source for the IGM if the IGM gas is colder than the CMB ($T_m < T_{\text{CMB}}$), otherwise the IGM gas would transfer energy into the CMB environment. The coupling between IGM gas and the CMB photons can be important when the difference between T_m and T_{CMB} is significant (Weymann 1965; Tegmark et al. 1997; Seager et al. 2000)

$$\left(\frac{dT_m}{dt} \right)_{\text{comp}} \approx k_{\text{comp}} T_{\text{CMB}}^4 x_{\text{ion}} (T_{\text{CMB}} - T_m), \quad (44)$$

where the coupling rate coefficient $k_{\text{comp}} \simeq 5.0 \times 10^{-22} \text{ s}^{-1}$.

Other IGM cooling terms are dominated by the adiabatic cooling during the expansion of the universe as

$$\left(\frac{dT_m}{dz} \right)_{\text{ad}} = \frac{2T_m}{1+z}, \quad (45)$$

for low temperature. Note that the IGM temperature will decrease independently as $T_m \propto (1+z)^2$ for a pure adiabatic cooling process. Furthermore, for sufficient high temperature $\sim 10^4$ K, the molecular hydrogen H_2 cooling will also be important. This cooling term can be calculated as

$$\left(\frac{dT_m}{dt}\right)_{H_2} = \Lambda_{H_2}(1 - x_{\text{ion}} - 2f_{H_2})f_{H_2}[n_A(1+z)^3]^2, \quad (46)$$

where we adopt the specific cooling coefficient Λ_{H_2} from Hollenbach & McKee (1979) and Yoshida et al. (2006). We neglect other chemical cooling processes such as Bremsstrahlung, helium line cooling, H_2 line cooling and hydrogen three-body reaction. HD cooling is important for $T < 200$ K and low density (Yoshida et al. 2006), but the gas adiabatic cooling will be dominated in this case. As we mainly pay attention to the evolution of the ionized fraction x_{ion} and IGM temperature T_m , we only include the evolution of hydrogen (H , H^- , H^+ , H_2) and electron gas (e^-) as the main species for ionization. More detailed simulation including other species and cooling processes is beyond our purpose of this paper. The evolution of the H_2 fraction is adopted from the semi-analytic model in Tegmark et al. (1997)

$$\frac{df_{H_2}}{dt} = k_m n_A (1+z)^3 (1 - x_{\text{ion}} - 2f_{H_2}) x_{\text{ion}}, \quad (47)$$

where we follow Tegmark et al. (1997) and Galli & Palla (1998) to calculate the reaction coefficient k_m .

3.2 Solutions of IGM Evolution

Since no direct evidence related to the UCMH radiation has been confirmed until now, the UCMH abundance is still uncertain. In this paper we take the UCMH fraction f_{UCMH} as a free parameter. In Fig. 2 we show the ionization fraction $x_{\text{ion}}(z)$ and the IGM temperature T_m for $f_{\text{UCMH}} = 10^{-4}$ and 10^{-6} , which correspond to today's expected abundance $\sim 1\%$ and 10^{-4} respectively. Moreover general discussion on the UCMH abundance will be given later. The initial x_{ion} at $z = 1000$ is adopted as 0.01, and T_m as the CMB temperature (Galli & Palla 1998; Ripamonti 2007; Ripamonti et al. 2007a,b). The first basic conclusion which is similar to the previous works is that, lighter dark matter particles or higher UCMH abundance give larger x_{ion} and higher T_m . An extreme bright UCMH annihilation background (e.g., $m_\chi c^2 \leq 1$ GeV for $f_{\text{UCMH}} \simeq 10^{-4}$ or $m_\chi c^2 \leq 100$ MeV for $f_{\text{UCMH}} \simeq 10^{-6}$), even gives a monotonically increased x_{ion} and $T_m \geq 10^4$ K without a standard reionization epoch in the early Universe. We compare the UCMHs annihilation results with the homogenous background annihilation, note that the homogenous dark matter annihilation background only produce noticeable effects for light dark matter particles $m_\chi c^2 < 1$ GeV or sterile neutrinos. UCMHs, which provide a new dominated dark matter annihilation gamma-ray background as showed in Section 2.1, play a more important role to ionize and heat the early Universe.

Furthermore, as the cosmological Jeans mass m_J can be taken as an indicator of the IGM structure evolution, the left panel of Fig. 3 gives the evolution of Jeans mass in the cosmic UCMH annihilation background. The Jeans mass $m_J \propto T_m^{3/2} \rho^{-1/2}$ should be a constant if the gas temperature is always equal to the CMB temperature $T_m = T_{\text{CMB}}$. In this paper we call this constant as ‘‘CMB mass’’. In the left panel of Fig. 3, m_J with various T_m is generally normalized in the unit of ‘‘CMB mass’’. The remaining Thomson scattering optical depth contributed by UCMH annihilation is showed in the right panel of Fig. 3. For

$6 \leq z < 30$, the remaining CMB optical depth is estimated as $\delta\tau \simeq 0.046 \pm 0.016$ by the WMAP five-year measurement.² We assume a linear increase of x_{ion} from $z = 10$ to the full ionization time $z = 6$, thus the upper bound contribution of UCMH annihilation to the measurable CMB optical depth is $\delta\tau \simeq 0.028 \pm 0.016 \leq 0.044$. Based on this consideration, in our examples only one extreme case that $m_\chi c^2 = 100$ MeV with $f_{\text{UCMH}} = 10^{-4}$ is ruled out by the CMB remaining optical depth in Fig. 3. UCMH annihilation can significantly increase the Thomson optical depth in the early Universe $z \gg 100$ up to $\delta\tau \sim 0.5$ without stringent constraints by the CMB optical depth measurement at $z < 30$. After the last-scattering epoch the ionization fraction x_{ion} can change from $x_{\text{ion}} \sim 10^{-4}$ (without dark matter annihilation) to a upper bound $x_{\text{ion}} \sim 0.1$ (e.g., $m_\chi c^2 = 1$ GeV and $f_{\text{UCMH}} = 10^{-4}$). Also, the IGM can be heated from a temperature T_m of adiabatically cooling $T_m \propto (1+z)^2$ in the absence of heating source to the upper bound $T_m > 10^3$ K with a sufficient amount of heating contributed by UCMH annihilation. A much higher Jeans mass than the ‘‘CMB mass’’ by $\sim 2 - 3$ orders of magnitude increase can be obtained due to the hotter IGM temperature. Therefore, we can natively estimate that the formation of small baryonic objects can be strongly suppressed, although more investigations need to be carried out in Section 4.

In general, we find the impact of UCMH annihilation on the IGM evolution can be empirically estimated by the factor $m_{\chi,100}^{-1} f_{\text{UCMH}}$, while the threshold of UCMH abundance to affect the IGM evolution is approximately given by $m_{\chi,100}^{-1} f_{\text{UCMH}} > 10^{-6}$, with an upper bound constrained by the CMB optical depth at late times $z < 30$ as $x_{\text{ion}} \sim 0.1$ and $T_m \sim 5000$ K at $m_{\chi,100}^{-1} f_{\text{UCMH}} \sim 10^{-2}$. The CMB optical depth enhancement at early times $z > 30$ can be more dramatic than the late times due to the higher annihilation luminosity in early redshift (equation 6), which is different from the PBH radiation which has higher luminosity at late times (Section 2.2.3; Ricotti et al. 2008). Further phenomenological constraints should be made by CMB polarization anisotropies, which is left for a future investigation. Keep in mind another channel to concentrate dark matter rather than primordial density perturbation is the formation of the first dark objects, which should affect the IGM evolution much later ($z < 100$) than UCMHs. Therefore UCMH annihilation has a definitely much earlier and more important impact on the IGM evolution from the last scattering to the structure formation time.

So far we give the results only for UCMH dark matter annihilation. Whether the X-ray emission from the PBH host UCMHs will significantly change the above results mainly depends on the fraction of PBH f_{PBH} , the average inflow radiation efficiency η and the critical redshift z_m as given in Section 2.2. In our paper we combine the factor ηf_{PBH} as one. Remember the results in Section 2.2: when X-rays from the center PBH region successfully passes

² The WMAP five-year measurements give the CMB Thomson scattering optical depth $\tau \simeq 0.084 \pm 0.016$ (Komatsu et al. 2009), which is mostly due to ionization at late times $z < 30$ (Ricotti et al. 2008; Natarajan & Schwarz 2010). If we subtract the optical depth contributed by the totally ionized gas $\tau(z \leq 6) = 0.038$, the remaining depth is $\delta\tau \simeq 0.046 \pm 0.016 \leq 0.062$ (Cirelli et al. 2009).

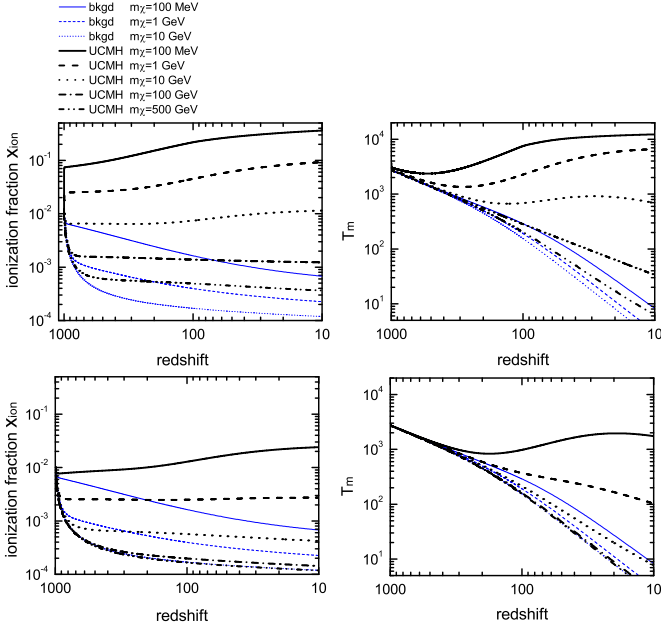


Figure 2. Effects of UCMH dark matter annihilation on the IGM evolution. Upper two panels correspond to the case of $f_{\text{UCMH}} = 10^{-4}$ and lower to $f_{\text{UCMH}} = 10^{-6}$. The thick (black) lines from the top down show the results for UCMH annihilation with $m_\chi c^2 = 100$ MeV, 1 GeV, 10 GeV, 100 GeV and 500 GeV, while the thin (blue) lines give the results of homogeneous dark matter background annihilation background for $m_\chi c^2 = 100$ MeV, 1 GeV and 10 GeV.

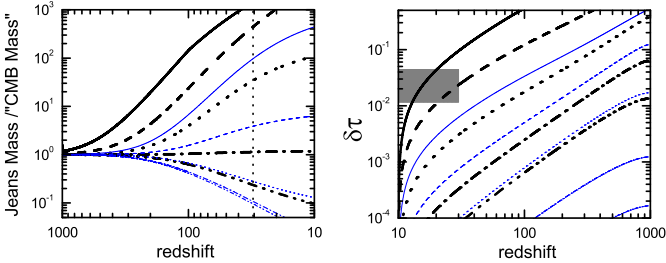


Figure 3. Left: ratio of Jeans mass to the “CMB mass”, which is the Jeans mass for the gas temperature always being equal to the CMB temperature. Right: evolution of the remaining Thomson scattering optical depth $\delta\tau$ with gray belt showing the WMAP 5-year 1σ of remaining CMB optical depth at $10 \leq z < 30$. The thick (black) lines are for $f_{\text{UCMH}} = 10^{-4}$ and thin (blue) for $f_{\text{UCMH}} = 10^{-6}$. The lines with same color from the top down are for $m_\chi c^2 = 100$ MeV to 500 GeV as in Fig. 2.

through the transparent baryon medium in the host UCMH at $z < z_m$, the much brighter X-ray luminosity and much larger interacting cross section $\sigma_{\text{tot}}(E_X)$ compared to the annihilation luminosity and $\sigma_{\text{tot}}(E_\gamma)$ usually guarantees the X-ray emission to be dominated over the UCMH annihilation (equations 15), except for a much lower PBH fraction

f_{PBH} below the value in equation (16). We will give a lower limit of f_{PBH} , above which X-rays have obvious impact on the IGM evolution at $z < z_m$. In the following calculation we assume equation (16) is always satisfied, and do not distinguish the redshift which divide the UCMH radiation into annihilation dominated or X-ray radiation dominated from the redshift which gives a transparent baryon environment in UCMHs, but simply use one parameter z_m .

In Fig. 4 we take z_m and ηf_{PBH} as parameters with the characteristic emission frequency as $E_X = 1$ keV, 10 keV and 100 keV, which correspond to the typical PBH mass as $10^2 M_\odot$, $10^{-2} M_\odot$ and $10^{-6} M_\odot$ respectively. Higher z_m means higher ratio $\delta m/M_{\text{PBH}}$ or lighter dark matter particles. Only X-ray emission as the energy source is calculated in this figure³. As showed in Fig. 4, the final properties of the IGM at $z \sim 10$ with same ηf_{PBH} and E_X are more or less closed to each other regardless the value of z_m , which means lower z_m gives more dramatic thermal and chemical change at $z < z_m$. According to equation (34), lower z_m corresponds to lighter m_χ , which also increase the UCMH annihilation. On the other hand, x_{ion} and T_m vary for more than three orders of magnitude from $E_X \sim 100$ keV ($10^{-6} M_\odot$) to $E_X \sim 1$ keV ($10^2 M_\odot$) with the same ηf_{PBH} , which means massive PBH favors the IGM ionization. On the other hand, the X-ray radiation effect can be neglected when $\eta f_{\text{PBH}} \leq 10^{-11}$ for $E_X \sim 100$ keV, but a smaller limit $\eta f_{\text{PBH}} \leq 10^{-12}$ is applied for $E_X \sim 1$ keV. Below the lower limit the PBHs are not expected to have any promising effects on reionization. The estimate in Fig. 5 shows that no strict constraints are made for $\eta f_{\text{UCMH}} \leq 10^{-7}$ by the remaining CMB depth $\delta\tau$, which allows a dramatically increased Jeans mass due to the hot IGM gas $\sim 10^4$ K.

As a result, X-ray emission from PBHs gives a more promising impact on the IGM evolution if $\eta f_{\text{PBH}} \gg 10^{-11}$ (10^{-12}) for $M_{\text{PBH}} \sim 10^{-6} M_\odot$ ($10^2 M_\odot$), or empirically to say, $\eta f_{\text{PBH}} \gg 1.8 \times 10^{-12} (M/M_\odot)^{-1/8}$. As we assume $f_{\text{UCMH}} \leq 10^{-4}$, we expect the UCMH dark matter annihilation only played its role on the IGM evolution at very high redshift $z_m < z < 1000$, but X-ray emission changes the Universe reionization history dramatically at relatively lower redshift $z < z_m$. Considering $\eta \sim 0.1$, the upper bound value $f_{\text{PBH}} \leq 10^{-6}$ is two orders of magnitude higher than the upper PBH abundance $\leq 10^{-8}$ in Ricotti et al. (2008) for $M_{\text{PBH}} > 10^3 M_\odot$, but much lower than the low mass PBH abundance constraint in Ricotti et al. (2008). How-

³ The more realistic case is that both z_m and E_X are the functions of the mass of PBH and its host UCMH, thus in principle neither z_m nor E_X are single free parameters. The real X-ray radiation background due to the PBH accretion happens at a certain z_m as showed in equations (28) and (34), and change its spectral energy distribution as a function of redshift (Ripamonti et al. 2008). Technically it is able to calculate the X-ray emission variation by introducing the initial mass function of PBHs and the host UCMHs. However, both of these two initial mass functions are poorly known. More elaborate models only make our model more complicated and uncertain. What we focus on in our calculations is the key differences between X-ray radiation and the much earlier occurred UCMH annihilation, so we only use the characteristic energy E_X , and the ratio $\eta f_{\text{PBH}}/f_{\text{UCMH}}$ to show the importance of the X-ray radiation. More discussion of PBH spectral energy distribution can be seen in Section 5.3.

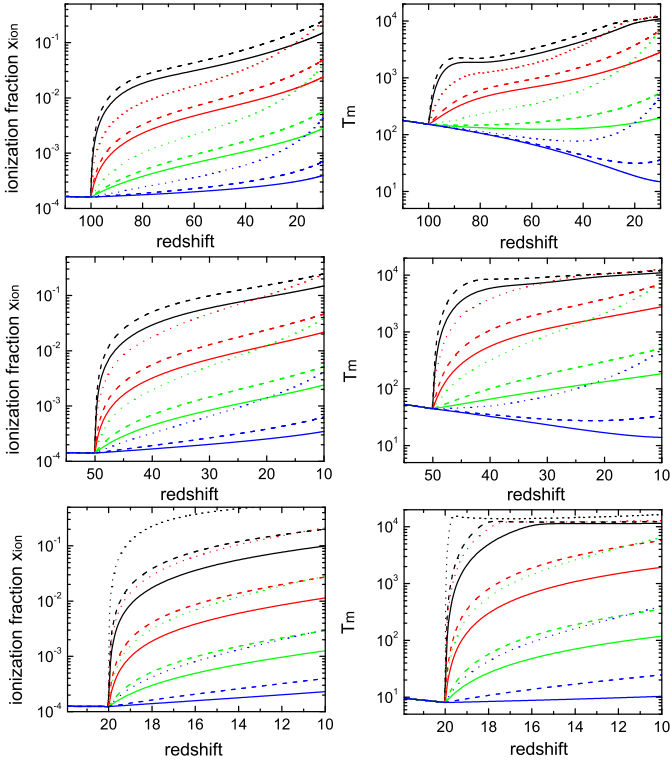


Figure 4. Effects of gas accretion around PBHs on the IGM ionization and temperature evolution. The upper panels are for the X-ray energy injection starting at $z_m = 100$, middle panels for $z_m = 50$ and lower for $z_m = 20$. The PBH fraction $\eta f_{\text{PBH}} = 10^{-7}$ (black lines), 10^{-8} (red lines), 10^{-9} (green lines) and 10^{-10} (blue lines). Characteristic emission energy are 100 keV (solid lines), 10 keV (dashed lines) and 1 keV (dotted lines).

ever, the massive PBH abundance constraint in Ricotti et al. (2008) is made by the Compton y -parameter estimate at $z_{\text{rec}} < z < z_{\text{eq}}$ without local UCMH trapping, while we consider the two-step accretion first by the host UCMHs and then by the center PBHs as mentioned in Section 2.2.3, X-rays can just locally heat the accreted gas inside UCMHs but not the entire cosmic gas at high redshift.

The abundance of IGM molecular hydrogen f_{H_2} in various UCMH radiation models is shown in Fig. 6 in this section. We see that when the UCMH energy injection can be neglected, this fraction goes back to $f_{\text{H}_2} \sim 10^{-6}$, which is consistent with the standard result (e.g., Galli & Palla 1998 and references therein). The upper bound of enhanced f_{H_2} is $f_{\text{H}_2} \sim 10^{-3}$, either due to the allowed UCMH dark matter annihilation constrained by the CMB optical depth, or the X-ray emission at $z_m \leq 100$.

4 FIRST STRUCTURES

In the hierarchical cold dark matter (CDM) scenario, the first cosmological objects are dark matter haloes, which are formed by gravitational instability from the scale-free density fluctuations (e.g., Green et al. 2005; Diemand et al.

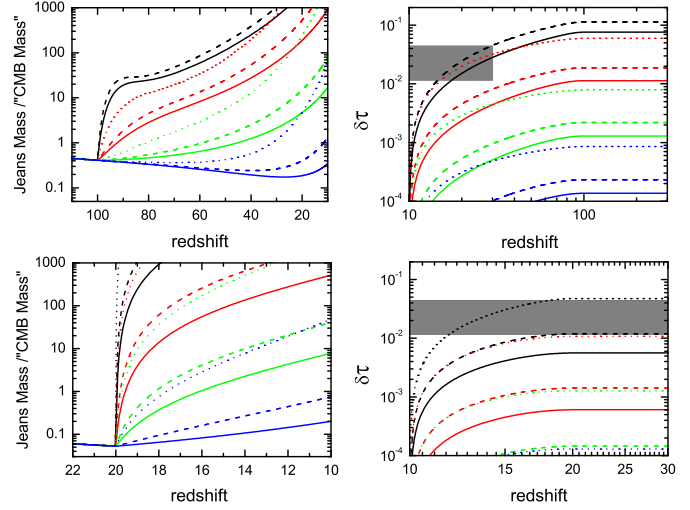


Figure 5. Ratio of Jeans mass to the “CMB mass” (left panels) and evolution of Thomson scattering depth (right panel) for the starting injection redshift $z_m = 100$ (upper panels) and 20 (low panels). The lines are as the same in Fig. 4.

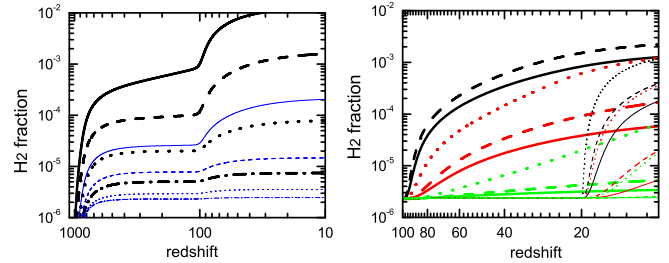


Figure 6. H_2 abundance evolution for UCMH annihilation (left panel) and gas accretion onto PBHs (right panel). The lines in the left are the same as in Fig. 3. The lines in the right panel are the same as in Fig. 4, but thick and thin are for $z_m = 100$ and $z_m = 20$ respectively.

2005; Yoshida 2009). The formation of the first baryonic objects depends on the detailed gas dynamical processes. The first baryonic objects can successfully collapse and form inside dark haloes when its cooling timescale for dissipating the kinetic energy is much shorter than the Hubble time. Tegmark et al. (1997) showed that the formation of the baryonic structure crucially depends on the abundance of the molecular hydrogen f_{H_2} . Biermann & Kusenko (2006) considered that the photons emitted by dark matter annihilation or decay inside the halo can boost the production of H_2 , and may favor the formation of the first structure. On the other hand, a different conclusion that the dark matter annihilation or decay can slightly delay the first baryonic structure formation was given by Ripamonti et al. (2007b). As they discussed, the higher central density in the baryonic cloud without dark matter energy injection could compen-

sate the lower abundance of H_2 and still lead to the fastest cooling. Nevertheless, no matter promotion or suppression caused by halo extended dark matter annihilation or decay, such effects are pretty small.

UCMHs can also be captured by the first dark matter objects, in this case the UCMH radiation can be much brighter than that from the extended large dark matter halo, even the fraction of UCMHs in the dark halo is tiny. In this section we focus on the dark halo structures with mass $\sim 10^6 M_\odot$ (or $10^7 M_\odot$ in the PBH heating case), as they favor the later first star formation (Broom et al. 2009; Yoshida 2009). For a typical $10^6 M_\odot$ halo in the early Universe, $\sim 10^{20}$ (10^{18}) or $\sim 10^8$ (10^6) UCMHs within this halo can be expected for an initial UCMH fraction $f_{\text{UCMH}} \sim 10^{-4}$ (10^{-6}) if the seed of UCMHs are generated in the electroweak or QCD phase transitions respectively (Scott & Sivertsson 2009). In these cases the UCMH emission can also provide a new type of radiation background in the dark halo. However, the uniform UCMH distribution treatment will break down if the number of massive UCMHs in a halo is less than ~ 10 . This happens for the massive UCMH case that $f_{\text{UCMH}} M_{\text{DM}}/m_h \leq 10$. In this section we study the effects of UCMH radiation on the first structure formation and evolution with $f_{\text{UCMH}} M_{\text{DM}} \gg m_h$, the case of only-several-luminous-UCMH will be discussed separately in Section 5.4 as a supplementary. As the virial temperature of $\sim 10^6 M_\odot$ haloes is less than the threshold for atomic hydrogen line cooling, these haloes are often referred as “minihalo” in literatures. However, for clearly, in this paper we call the first dark matter structure as (cosmological) dark matter haloes or dark haloes, which should not be confused with the UCMHs.

4.1 Dark Matter Annihilation

The profiles of the cosmological dark matter haloes are chosen before our calculation. The equations for the halo profile are listed in the Appendix. Before the formation of the first stars, the energy injection inside a large dark matter halo mainly contributed by the local emission from the UCMHs in the halo, the local annihilation or decay of the extended dark matter within the halo, and the outside radiation background which injects into the halo. We check the total energy produced by dark matter annihilation with a dark halo as $L_{\text{halo}} = L_{\text{UCMH}} + L_{\text{ext}}$, with L_{UCMH} and L_{ext} being the annihilation luminosity from UCMHs and the extended dark matter in this halo. The typical ratio $L_{\text{UCMH}}/L_{\text{ext}}$ is demonstrated in Fig. 7, where we adopt an isothermal dark halo model and $f_{\text{UCMH}} = 10^{-6}$. We find both L_{UCMH} and L_{ext} are proportional to the total halo mass M_{DM} , so $L_{\text{UCMH}}/L_{\text{ext}}$ is independent to M_{DM} . In Fig. 7 L_{UCMH} is mostly dominated in the halo, except for large z_{vir} with light dark matter particles (e.g., < 10 GeV for $f_{\text{UCMH}} = 10^{-6}$ and $z_{\text{vir}} = 100$, much lighter dark matter particles is required for more abundant UCMHs or smaller z_{vir}). Therefore, similar to the IGM environment, the energy injection mechanism inside a dark halo which contains UCMHs can be very different from the no-UCMH case. We focus on the ionization and heating inside the dark matter halo. Also, we mention that the results for $L_{\text{UCMH}}/L_{\text{ext}}$ in NFW haloes are very similar to the isothermal haloes in Fig. 7.

The simple criterion of baryonic matter filling in a dark

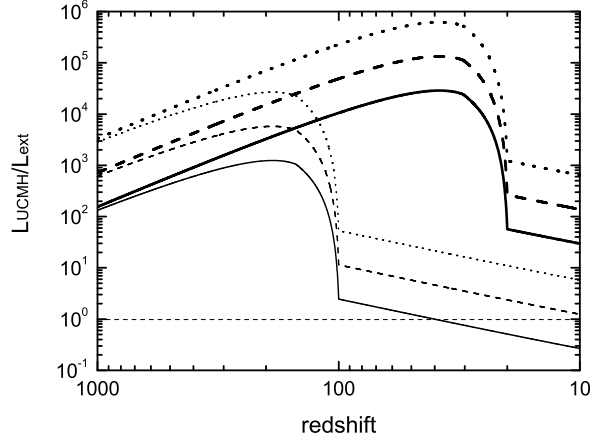


Figure 7. Ratio between L_{UCMH} and L_{ext} for $m_\chi c^2 = 1$ GeV (solid lines), 10 GeV (dashed lines), 100 GeV (dotted lines) and isothermal extended dark matter halo. Thick and thin lines correspond to the virial redshift $z_{\text{vir}} = 20$ and 100 respectively. The UCMH fraction is adopted as $f_{\text{UCMH}} = 10^{-6}$. The case of $L_{\text{UCMH}} = L_{\text{ext}}$ is marked as the horizon thin dashed line.

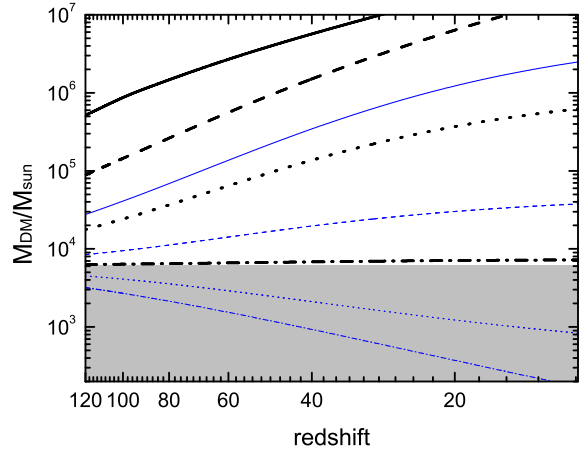


Figure 8. The minimal dark halo mass for $T_m = T_{\text{vir}}$ with the IGM heated by UCMHs. The shaded area is for the case that the minimal halo mass for gas collapsing becomes $M_{\text{DM}} < 6.1 \times 10^3 M_\odot$ due to a lower ambient gas temperature compared to the CMB temperature. The lines from $m_\chi c^2 = 100$ MeV to 500 GeV as in Fig. 3.

halo is approximately taken as the IGM gas temperature being cooler than the virial temperature of the halo $T_m < T_{\text{vir}}$, otherwise the gas pressure prevents the gas from collapsing. We do not include the temperature cooling slope criterion as in Tegmark et al. (1997) to further study the baryon cooling and collapsing in the dark halo. Fig. 8 gives the dark matter halo mass for the critical case $T_m = T_{\text{vir}}$ with UCMH annihilation heating the ambient IGM gas. Generally more massive dark halo mass is needed for gas filling into

dark haloes and forming baryonic structure in the haloes. If $T_m = T_{\text{CMB}}$ the minimum halo mass for gas filling is $6.1 \times 10^3 M_\odot$, while the minimum halo mass increases significantly for $T_m \gg T_{\text{CMB}}$. In this sense, the formation of the first baryonic objects will be obviously suppressed in the small dark haloes located in host IGM gas. However, in the pure UCMH annihilation case without PBH radiation, we expect $\sim 10^6 M_\odot$ dark haloes attract baryons at $z > 10$ in most cases expect for $f_{\text{UCMH}} m_\chi^{-1} \geq 10^{-2}$.

The annihilation energy deposited in a dark halo can be linearly divided into two parts: the energy from the background where the cosmic UCMH annihilation occurs $\epsilon_{\text{bgd}}(z)$, and that within the local dark halo $\epsilon_{\text{loc}}(z)$. The term $\epsilon_{\text{bgd}}(z)$ is obtained by equation (39). The local energy $\epsilon_{\text{loc}}(z)$ is a function of position inside the halo. We focus on the energy deposition at the center of the halo. The contribution by the extended dark matter in an isothermal halo is

$$\epsilon_{\text{loc,iso}}(z) = \frac{\langle \sigma v \rangle c^2 (1 - f_\chi)}{2 \mu m_p m_\chi f_\chi} \sigma_{\text{tot}}(E_\chi) \rho_{\text{core}}^3 \left(\frac{6}{5} R_{\text{core}} - \frac{R_{\text{core}}^6}{5 R_{\text{tr}}^5} \right), \quad (48)$$

where $f_\chi = \Omega_{\text{DM}}/\Omega_{\text{M}} \approx 0.833$. On the other hand, the local energy deposited by the UCMH annihilation depends on the UCMH distribution inside the halo. If we assume the UCMHs number density is uniformly distributed depending on the halo mass density, i.e., $\frac{dn_{\text{UCMH}}(r)}{dM_{\text{DM}}(r)} \propto \text{const.}$ (a relevant distribution simulation see Sandick et al. 2011), we have

$$\begin{aligned} \epsilon_{\text{loc,UCMH}}(z) &\simeq \frac{L_{\text{UCMH}} \sigma_{\text{tot}}(E_\chi) (1 - f_\chi)}{\mu m_p f_\chi M_{\text{DM}}} \int_0^{R_{\text{tr}}} \rho^2 dr \\ &\simeq \frac{L_{\text{UCMH}} \sigma_{\text{tot}} \rho_{\text{core}}^2 (1 - f_\chi)}{\mu m_p M_{\text{DM}} f_\chi} \left(\frac{4}{3} R_{\text{core}} - \frac{R_{\text{core}}^4}{3 R_{\text{tr}}^3} \right). \end{aligned} \quad (49)$$

In the following calculation we adopt equation (49) for UCMH annihilation, and also include the extended dark matter annihilation within the halo.

Figure 9 shows the gas evolution at the center of an $10^6 M_\odot$ isothermal halo virializing at $z_{\text{vir}} = 20$ or $z_{\text{vir}} = 100$. We also show the protohalo stage at $z > z_{\text{vir}}$. More energetic annihilation due to larger f_{UCMH} or lower m_χ gives higher x_{ion} and f_{H_2} . The UCMH annihilation gives a significant impact on T_m before virialization in the protohalo stage, that is because the cooling and heating mechanisms are different before and after virialization. The change of T_m before virialization is mainly due the heating by background UCMH annihilation, which is totally dominated over the extended dark matter annihilation, thus brighter UCMH annihilation luminosity gives a higher gas temperature at $z > z_{\text{vir}}$. However, after a dramatic temperature increase during the virializing $z \sim z_{\text{vir}}$, H_2 cooling becomes the main process to cool the denser gas at $z < z_{\text{vir}}$. The peak temperature during virializing is around $\sim 1000 - 2000$ K. We find that higher H_2 abundance, which is caused by brighter UCMH annihilation, gives a lower gas temperature after virialization for small z_{vir} (~ 20), but a higher temperature for large z_{vir} (~ 100). This result is just between that in Biermann & Kusenkov (2006), who considered the effects of sterile neutrino decay can favor the structure formation, and Ripamonti et al. (2007b), who showed that dark matter annihilation will slight delay the structure formation. The main reason of our difference from Ripamonti et al. (2007b) for $z_{\text{vir}} \ll 100$ is that, we take the baryon gas density to be proportional to the halo density $n_b \propto \rho$ as in Tegmark et al. (1997), therefore more molecular gas due to stronger heating just means more efficient

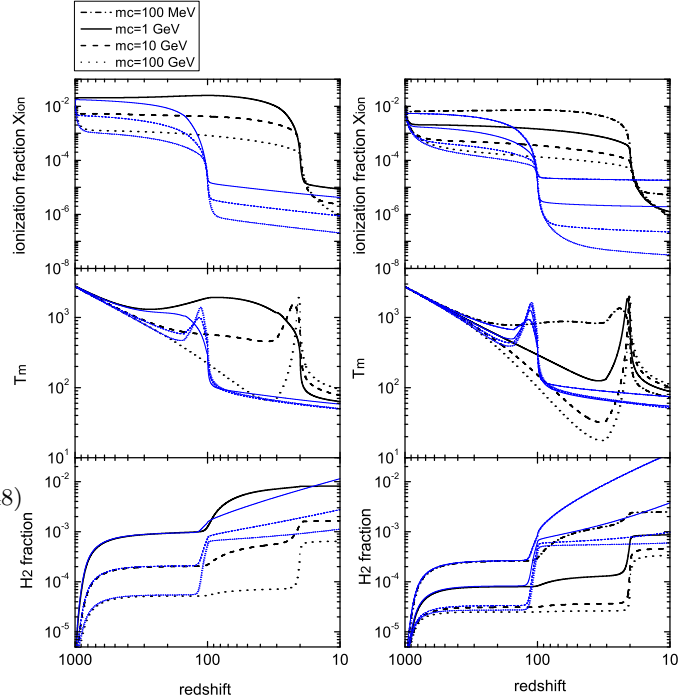


Figure 9. Effects of UCMH and extended dark matter annihilation inside an $10^6 M_\odot$ isothermal halo on the evolution of ionization (upper panels), temperature (middle panels) and H_2 fraction f_{H_2} (lower panels) at the central region of the halo, where we choose the virial redshift $z_{\text{vir}} = 20$ (thick black lines) and 100 (thin blue lines), $m_\chi c^2 = 100$ MeV (dash-dotted lines), 1 GeV (solid lines), 10 GeV (dashed lines) and 100 GeV (dotted lines).

cooling. A more elaborate result can be made by adding more detailed gas dynamics and energy transfer including the UCMH radiation within the halo (Tegmark et al. 1997; Ripamonti et al. 2007b). But such a new calculation should not change the fact that UCMH radiation, as well as the extended dark halo annihilation, cannot change the gas temperature in the halo obviously after virialization.

Note that the temperature T_m in the halo only change by a factor of ~ 3 for a several orders of magnitude change to the UCMH annihilation luminosity inside the halo. Therefore, we cannot expect the first baryonic structure formation can be obviously promoted or suppressed. After virialization, the effects of dark matter annihilation are always secondary compared to the H_2 cooling mechanism. On the other hand, gas chemical properties such as x_{ion} and f_{H_2} can be changed significantly that higher x_{ion} and f_{H_2} are produced by brighter dark matter annihilation.

4.2 Gas accretion onto PBHs and X-ray Emission

If we consider gas accretion onto PBHs, and take the PBH fraction as $\eta f_{\text{PBH}} > 10^{-11}$ (10^{-12}) for $M_{\text{PBH}} = 10^{-6} M_\odot$ ($10^2 M_\odot$), the first baryonic structure formation will be different. Fig. 10 shows the minimal dark matter mass for the critical case $T_m = T_{\text{vir}}$ with different ηf_{PBH} and the characteristic radiation $E_\chi = 10$ keV. Different from the dark

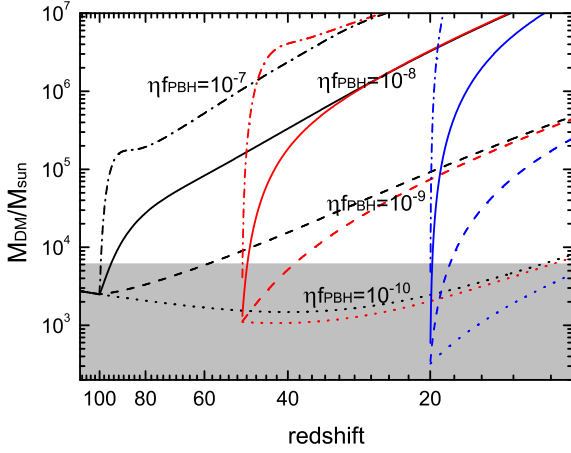


Figure 10. The minimal dark halo mass at $T_m = T_{\text{vir}}$ for PBH radiation with $\eta_{\text{PBH}} = 10^{-7}$ (dash-dotted lines), 10^{-8} (solid lines), 10^{-9} (dashed lines), 10^{-10} (dotted lines) and $z_m = 100$ (dark lines), 50 (red lines) and 20 (blue lines). The characteristic PBH radiation is $E_X = 10$ keV. The shaded area is for the case that the minimal halo mass for gas collapsing becomes $M_{\text{DM}} < 6.1 \times 10^3 M_\odot$ due to a lower ambient gas temperature compared to the CMB temperature.

matter annihilation heating case (Fig. 8), the minimal dark halo mass dramatically increase after z_m . For $z_{\text{vir}} = 20$, the minimal dark haloes increase to $> 10^6 M_\odot$ for $\eta_{\text{PBH}} \geq 10^{-8}$. Moreover, if we combine the annihilation before z_m with the X-ray emission after z_m , the minimal dark halo mass for $T_m = T_{\text{vir}}$ can be even larger.

Moreover, we expect the gas accretion onto PBHs in the dark halo environment above the critical mass in Fig. 10 will be slightly different from that in the ambient IGM, because the baryon gas is denser within a dark halo than the ambient IGM, which leads to a different accretion rate and baryon fraction inside UCMHs compared to the IGM-located-UCMHs. The accretion rate \dot{M}_{UCMH} and baryon fraction f_b inside a PBH host UCMH should be higher than those outside the halo. Therefore it is more difficult for X-rays from PBHs to pass through the host UCMH without absorption. The critical redshift z_m^{halo} for X-rays escaping from the UCMH baryonic environment should be slightly delayed inside the halo than that in the background $z_m^{\text{halo}} < z_m^{\text{bgd}}$. It is possible that in a period of time that X-ray energy injection and deposition within a halo is mainly from the background even after virialization.

The evolution of the baryonic structure inside a $10^7 M_\odot$ isothermal dark halo, as an example, is showed in Fig. 11. We consider two models: the number density of PBH host UCMHs being uniformly distributed per halo mass as mentioned in Section 4.1; also the uniformly distributed UCMHs per halo volume inside the halo as $\frac{dn_{\text{UCMH}}}{dV_{\text{halo}}} \propto \text{const.}$. Different UCMH distribution inside the halo would give different baryonic evolution. The local energy deposition for the UCMHs' uniform distribution per halo volume is written as

$$\epsilon_{\text{loc,acc}}(z) \simeq \frac{L_{\text{acc}} \sigma_{\text{tot}} E_X \rho_{\text{core}} (1 - f_X)}{\mu m_p f_X V_{\text{halo}}} \left[2R_{\text{core}} - \frac{R_{\text{core}}^2}{R_{\text{tr}}} \right], \quad (50)$$

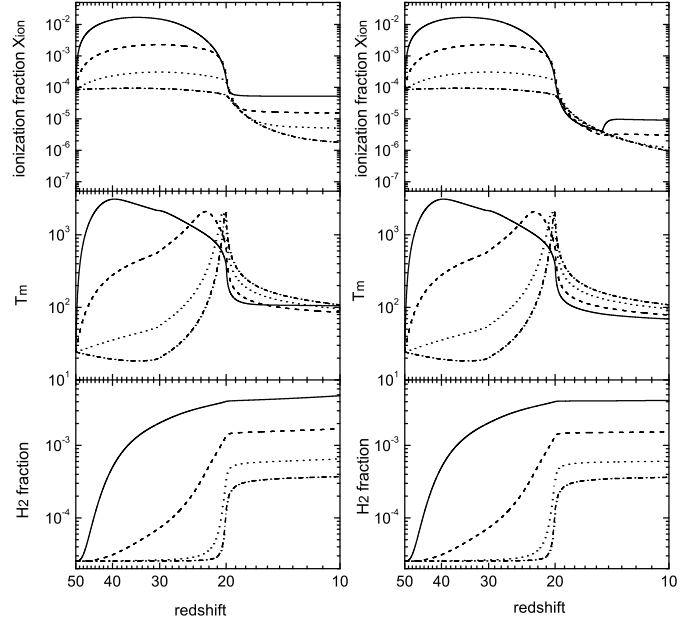


Figure 11. Effects of gas accretion onto PBH inside a $10^7 M_\odot$ isothermal halo with $z_{\text{vir}} = 20$, $z_m^{\text{bgd}} = 50$, $z_m^{\text{halo}} = 30$ (left panel) and $z_m^{\text{UCMH}} = 15$ (right panel). The characteristic $E_X = 10$ keV with $\eta_{\text{PBH}} = 10^{-7}$ (solid lines), $\eta_{\text{PBH}} = 10^{-8}$ (dashed line), $\eta_{\text{PBH}} = 10^{-9}$ (dotted lines), $\eta_{\text{PBH}} = 10^{-10}$ (dash-dotted lines). We choose a more massive halo $10^7 M_\odot$ because more massive haloes are favors for the structure formation in this case. In the left panel we take $\frac{dn_{\text{UCMH}}}{dM_{\text{halo}}}$ uniformly and right panel $\frac{dn_{\text{UCMH}}}{dV_{\text{halo}}}$ uniformly.

where L_{acc} is the total X-ray luminosity due to gas accretion onto PBHs inside the first baryonic object. The main results in Fig. 11 is very similar to those of dark matter annihilation in Fig. 9. For low virialization redshift $z_{\text{vir}} = 20$, the gas temperature is cooler for higher X-ray luminosity, but T_m inside the halo only changes by a factor of 2 to 4 for a four orders of magnitude change in the X-ray luminosity. An more obvious change of chemical quantities (x_{ion} , f_{H_2}) than the temperature change occurs for different X-ray luminosity within the halo. This means the effects of X-ray emission form PBHs on the gas evolution inside a halo is very small. PBHs which uniformly distribute per halo volume gives a slighter cooler gas within the halo, as well as lower x_{ion} and f_{H_2} than the uniformly distributed UCMHs per halo mass. That is because the latter model makes the average distance of UCMHs to be closer to the halo center, and gives more effects to change the gas properties at the center.

In summary, UCMH radiation including both annihilation and PBH gas accretion enhances the baryon chemical quantities such as x_{ion} and f_{H_2} inside dark matter haloes which above the minimal halo mass for $T_m = T_{\text{vir}}$, but the impact of UCMH radiation on the temperature of first baryonic objects is small (by a factor of several), which shows the change of first baryonic structure formation due to UCMH radiation is less important than the H_2 cooling and dark halo virialization time. However, the new chemical conditions provided by UCMH radiation can be more important

to affect the later gas collapse and first star formation after the first baryonic object formation, because more abundant H_2 and electrons acting as the cooling agents can cool the gas more efficient during the gas collapse process, and provide a lower fragmentation mass scale and first star mass (e.g., Stacy & Bromm 2007). As we mainly focus on the first baryonic structure formation and evolution, the detailed calculation of first star formation due to the changed gas chemical components should be investigated more detailed in the future.

5 DISCUSSION

5.1 Status of UCMH Radiation in Reionization, Other Sources

A variety of cosmological sources can reionize and heat the IGM at different redshifts before $z \simeq 6$. So far we showed that UCMHs, even merely occupy a tiny fraction of total dark matter mass, provide a new gamma-ray background for gas heating and ionization. Also, the X-ray emission from the accreting PBHs could change the IGM gas evolution history dramatically after $z_m \ll 1000$, where the value of z_m depends on the masses of PBH, host UCMHs and dark matter particles. Furthermore, we investigate that both dark matter annihilation and X-ray emission from UCMHs can dominate over the annihilation of extended dark matter halo. Therefore UCMHs are also an important energy source in dark matter haloes before the first star formation. In this section we briefly review all candidate energy sources during the Universe reionization era $10 \leq z < z_{eq}$. In particular, we emphasize the importance of UCMH radiation among all of these sources in different times.

In this paper we focus on the heating and ionization processes after the last scattering epoch $z \sim 1000$, but some interesting effects can be produced by primordial energy sources at earlier time $z > 1000$. For example, cosmic gas heating and CMB spectral distortion at $z_{rec} < z < z_{eq}$ produced by PBH gas accretion can be used to constrain the PBH abundance that $f_{PBH} \leq 10^{-8}$ for $M_{PBH} \geq 10^3 M_\odot$ in the absence of UCMH annihilation (Ricotti et al. 2008). However, as showed in Section 2.2, UCMH annihilation can be more important than PBH gas accretion in the very earlier Universe even though UCMHs are just beginning to grow at that time. Hotter cosmic gas heated by dark matter annihilation suppresses the PBH gas accretion to becomes the dominated sources to distort CMB, and even changes the cosmic recombination process as showed in Fig. 2. Compton y -parameter is likely to be used to constrain the UCMH abundance based on the annihilation scenario in future work.

The influence of dark matter annihilation or decay at $z \leq 1000$ on the IGM during the reionization era has been discussed by many authors (Chen & Kamionkowski 2004; Hansen & Haiman 2004; Pierpaoli 2004; Mapelli & Ferrara 2005; Padmanabhan & Finkbeiner 2005; Zhang et al. 2006; Mapelli et al. 2006; Ripamonti 2007; Yuan et al. 2010; Chluba 2010). Some authors also use the observation data to constraint the cross section of the dark matter interaction (Cirelli et al. 2009; Calli et al. 2009; Slatyer et al. 2009; Kanzaki et al. 2010). The basic assumption is that the dark matter distribution is smooth and homogenous at $z \geq 100$.

However, the annihilation power can be strongly increased by UCMHs in the early Universe, as what we have discussed in this paper.

The next commonly suggested sources of ionization and heating is the first dark objects (dark haloes), which formed approximately at $z \leq 100$. Dark matter haloes enhanced the overall cosmic dark matter annihilation density due to the dark matter concentration in haloes (Iliev et al. 2005; Oda et al. 2005; Ciardi et al. 2006; Chuzhoy 2008; Myers & Nusser 2008; Natarajan & Schwarz 2008; Belikov & Hooper 2009; Natarajan & Schwarz 2009; Natarajan & Schwarz 2010). The mass distribution of dark haloes varies from very low mass at ($\sim 10^{-6} M_\odot$) to high mass ($\sim 10^{12} M_\odot$) (Green et al. 2005; Diemand et al. 2005; Hooper et al. 2007), depending on the different damping scales due to different dark matter models (Abazajian et al. 2001; Boehm et al. 2005), as well as the mass-halo function (Press & Schechter 1974; Sheth & Tormen 1999). If UCMHs collapse with the homogenous dark matter together, the UCMH annihilation flux could still dominate over the total annihilation flux within the dark matter haloes, at least in massive dark haloes with $f_{UCMH} M_{DM} \gg m_h$. However, remember that small dark matter haloes contribute to a significant part of the total annihilation rate after structure formation. The profiles of the earth-mass dark matter haloes and the gamma-ray flux due to annihilation have also been studied recently (Diemand et al. 2005; Ishiyama et al. 2010). Similar to the UCMH emission, a large enhancement of annihilation signal is also expected due to the emission from the dark matter subhaloes as the remnant of structure formation at $z < 60$. Whether UCMHs or small haloes are more important for ionization and heat after $z \sim 60$ should be investigated in the future.

The following ionization sources are the accreting PBHs, which locate in their host UCMHs, as mentioned in Section 2.2. PBHs with host UCMHs lead to a faster accretion than naked PBHs, but also absorb the X-ray emission due to baryon accumulation within the UCMH. The PBH accreting could only be more important than UCMH annihilation at $z \leq z_m \ll 1000$ with sufficient abundance and radiation efficiency. Keep in mind that the X-ray emission here is from PBHs, or say, the PBH-UCMH systems, which play an earlier role than the so-called accreting “first black holes (BHs)”, which are the remnants of first stars at $z \sim 15$.

As mentioned in Section 4, dark matter annihilation or X-ray emission affects the baryonic structure formation and evolution. Also, they affect the process of first star formation. The standard first star formation carried out at $z \sim 20$ (Abel et al. 2002; Broom et al. 2009), but the first star forming history can be affected by the primordial magnetic fields (Tashiro & Sugiyama 2006), or by extended dark matter annihilation in the halo (so-called “dark star”, see Spolyar et al. 2008; Spolyar et al. 2009). Previously it was said that the first stars gave the first light to end the cosmic “dark age”, that cannot be true if exotic sources such as dark matter annihilation and accreting PBHs are included.

Next ionization sources are more familiar to us. First stars emitted UV light and produced the “ionized bubbles”, which could directly partially ionize the Universe at $z < 20$, or affected the coming formation of next generation stars and later galaxy formation (e.g., Haiman & Loeb 1997; Wyithe & Loeb 2003;

Shull & Venkatesan 2008; Whalen et al. 2010). The death of first stars, produced the “first generation BHs”, which emitted X-rays and ionized the Universe at $z \sim 15$ or even closer (Cen 2003; Ricotti & Ostriker 2004; Madau et al. 2004; Ripamonti 2007; Thomas & Zaroubi 2008). The reionization process was completed after galaxy formation, as galaxies are generally considered the main candidates for the reionization of the Universe at $z \sim 6$ (Meiksin 2009, and references therein).

Future work that can be done includes studying the heating and ionization processes at $z > 1000$ due to annihilation, comparing the total annihilation rate from small dark haloes ($10^{-6} M_\odot < M_{\text{DM}} < f_{\text{UCMH}}^{-1} m_h$ as we mentioned above) with that from UCMHs, and distinguish the impacts of different ionization sources using the CMB polarization anisotropies and 21 cm spectra observational constraints. Actually, CMB polarization and hydrogen 21 cm line are powerful potential probes of the era of reionization to constrain the early energy sources. The high multipoles of polarization anisotropies may be able to distinguish UCMHs from small dark structures formed at $z < 100$, and further constrain the UCMH and PBH abundances.

5.2 Different UCMH Profiles

Remember that in Section 2.1 although several UCMH annihilation rate due to various profiles were given in Fig. 1, we choose the UCMH profile as $\rho \propto r^{-9/4}$ with a cut off at $\rho_{\text{max}} \propto (t - t_i)^{-1}$. Such a profile is based on the analytical solution of the radial infall onto a central overdensity (Bertschinger 1985). A shallower density profile $\rho(r) \propto r^{-1.5}$ which is given if the central accretor is a black hole, or a steeper profile $\rho(r) \propto r^{-3}$ simulated by Mack et al. (2007), will change the total annihilation luminosity of a UCMH significantly. Fig. 12 gives an example of the different annihilation luminosity due to different density profiles in an entire UCMH. More concentrated dark matter distribution in a steeper profile leads to much higher total annihilation rate within the UCMH, because the center region of a UCMH contributes to most part of the total annihilation rate. However, we conclude that the overall cosmic annihilation luminosity density equation (10) will not be changed too much for two reasons. First of all, the $\rho \propto r^{-3}$ profile usually appears in the outer region of a UCMH, but the change of the UCMH density profile at the outer region $r \gg r_{\text{cut}}$ will not dramatically change the total annihilation rate, the density distribution at the central region is crucial to determine the total annihilation rate. Second, the contribution of PBH host UCMHs (with the profile $\rho(r) \propto r^{-1.5}$ near the center) to the overall cosmic annihilation should be much less important than the initial overdensity seeded UCMHs ($\rho(r) \propto r^{-2.25}$), both due to their shallower inner profile and the much lower abundance $f_{\text{PBH}} \ll f_{\text{UCMH}}$. The annihilation luminosity should still be taken into account if the dark matter particle inner trajectory is high eccentric with a much closer pericenter than the cut off radius as in equation (4), but it is still lower than the luminosity of the overdensity seeded UCMHs as showed in Section 2.1 (Lacki & Beacom 2010).

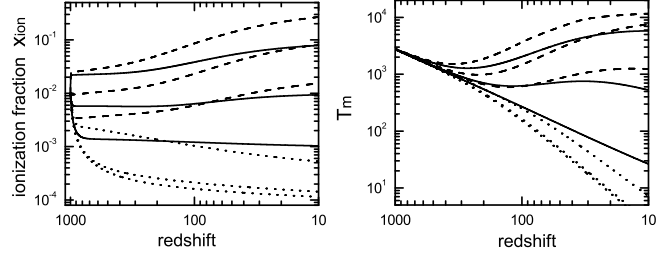


Figure 12. An example of IGM evolution caused by UCMH annihilation with different UCMH profiles. In order to see the effects more clearly, UCMH fraction is taken as $f_{\text{UCMH}} = 10^{-4}$. The same group of lines from the top down show the results for $m_\chi c^2 = 1$ GeV, 10 GeV and 100 GeV with $\rho \propto r^{-9/4}$ (solid lines), $\rho \sim r^{-3}$ (dashed lines) and $\rho \sim r^{-1.5}$ (dotted lines).

5.3 Extended Radiation Spectral Energy Distribution

In Section 3 the products of two dark matter particles annihilation are assumed to be two gamma-ray photons both with energy $m_\chi c^2$, and X-ray photons emitted from PBH host UCMHs are characterized with the single energy reflecting the center PBH mass $E_X \simeq 3 \text{ keV } (M_{\text{PBH}}/M_\odot)^{-1/4}$. The simplified treatment with a monochromatic (i.e., δ -function) spectrum of local UCMH emissivity is a good approach to demonstrate the crucial UCMH effects on the IGM evolution depending on the most crucial parameters such as UCMH and PBH abundances f_{UCMH} and f_{PBH} , as well as dark matter particle mass m_χ . In this section we will experiment other extended photon spectral energy distributions (SEDs) for UCMH radiation rather than δ -function, and study the dependence of UCMH emissivity with SED. We will see that more elaborate considerations can quantitatively change the ionization results, but will not change the basic conclusions of UCMH radiation qualitatively. We first adopt a power law spectrum as $F(E, z) \propto E^{-a}$, and then discuss another spectrum as $F(E, z) \propto E^b \exp(-dE)$, which are two most commonly used SEDs for annihilation and BH X-ray emission.

First of all we give an analytic calculation for UCMH radiation with locally monochromatic spectrum, based on an approximation that the optical depth described as equation (38) can be neglected $\tau \ll 1$. This condition is applied to the spectrum $E_\gamma(E_X) \gg 10 \text{ keV}$. Under the approximation $\tau \ll 1$ equation (37) in Section 3 can be simplified as

$$\frac{dn}{dE_\gamma} \simeq \frac{1}{E_0 E_\gamma} \frac{c}{H_0 \sqrt{\Omega_m}} \left(\frac{E_\gamma}{E_0} \right)^{\frac{1}{2}-\zeta} \frac{l(z)}{(1+z)^{3/2}}. \quad (51)$$

where the emitted photon number n and luminosity $l(z)$ can be applied to both annihilation ($n_{\text{ann}}, l_{\text{ann}}(z)$) or X-ray luminosity ($n_X, l_{\text{acc}}(z)$), E_0 for E_χ or E_X respectively, and $l(z) \propto (1+z)^\zeta$ with $\zeta \approx 4$ for annihilation and $\zeta \approx 3$ for X-ray emission. We take the interaction cross section between photons and the IGM gas as $\sigma_{\text{tot}}(E) \propto E^{-k}$. The total energy deposition per second per volume equation (40) is integrated as

$$\epsilon_\delta(z) = \frac{c}{H_0\sqrt{\Omega_m}} \left(\frac{13}{2} - \zeta - k \right)^{-1} l(z) n_A (1+z)^{3/2} \sigma_{\text{tot}}(E_0), \quad (52)$$

where the subscript δ is marked for monochromatic SED as in equation (40). For high energy gamma-ray photons we can take $k \approx 2$ for Klein-Nishina cross section but for X-ray photons we take $k \approx 0$ for $E_X \gg 1$ keV. Another thing we mention is that ionization rate $I(z) \propto \epsilon(z)$ for $x_{\text{ion}} \ll 1$, so we only track $\epsilon(z)$ based on different SEDs.

The first extended SED is $F(E, z) \propto E^{-1}$ for $E_1 \leq E \leq E_2$, which gives a spectral number density for $\tau \simeq 0$

$$\frac{dn}{dE_\gamma} \simeq \frac{c}{H_0\sqrt{\Omega_m}} \left(\frac{2}{13-2\zeta} \right) \frac{l(z)}{\ln \Lambda} (1+z)^{-3/2} E_\gamma^{-2}, \quad (53)$$

where $\Lambda = E_2/E_1$. Note that the number spectrum equation (53) is different from the equation (51) in the monochromatic SED case. If we consider dark matter annihilation $k \simeq 2$, the total energy deposition for UCMH annihilation is written as

$$\begin{aligned} \epsilon(z) &\simeq \frac{c}{H_0\sqrt{\Omega_m}} \left(\frac{2}{13-2\zeta} \right) \frac{l_{\text{ann}}(z)}{k \ln \Lambda} n_A (1+z)^{3/2} \\ &\times \left(\frac{E_0}{E_1} \right)^k \sigma_{\text{tot}}(E_0) \left(\frac{1+z_{\text{eq}}}{1+z} \right)^k. \end{aligned} \quad (54)$$

Compared with equation (52), the most obvious difference is the additional two factors $(E_0/E_1)^k$ and $(1+z_{\text{eq}})^k/(1+z)^k$ significantly increase the annihilation energy density if $E_0 \gg E_1$. However This energy amplification for power law SED might be overestimated as we take the lower limit of the energy (40) as $E_{\text{eq}} = E_1(1+z)/(1+z_{\text{eq}})$, i.e., the Universe at redshift z can receive the emission from the matter-radiation equality era. A more general expression $(E_1/E_i)^k$ can be used instead of $(1+z_{\text{eq}})^k/(1+z)^k$ with E_i being the threshold energy photons from UCMH radiation, then the amplified factor compared to equation (52) can be written as $(E_0/E_i)^k \gg 1$, no direct relation with E_1 and E_2 . On the other hand, for the X-ray emission from a PBH host UCMH, as $k \approx 0$ and the cross section is more or less the Thomson cross section, then the energy density is written as

$$\begin{aligned} \epsilon(z) &\simeq \frac{c}{H_0\sqrt{\Omega_m}} \left(\frac{2}{13-2\zeta} \right) l_{\text{acc}}(z) n_A (1+z)^{3/2} \sigma_T \\ &\times \left[1 + \ln \left(\frac{E_1}{E_i} \right) / \ln \Lambda \right] \end{aligned} \quad (55)$$

In this case the energy density can be increased compared to the monochromatic spectrum if $E_1 > E_i$, or decreased for $E_1 < E_i$. But the logarithmic enhancement $\ln(E_1/E_i)$ in X-ray emission case is less significant than the annihilation case.

For a more general power law spectrum $F(E, z) \propto E^{-a}$ ($E_1 \leq E \leq E_2$) with $a > 1$, the number density spectrum and energy deposition are calculated as

$$\frac{dn}{dE_\gamma} \simeq \frac{c}{H_0\sqrt{\Omega_m}} \left(\frac{a-1}{a+\frac{11}{2}-\zeta} \right) (1+z)^{-3/2} \left(\frac{E_1}{E_\gamma} \right)^a \frac{l(z)}{E_1 E_\gamma}, \quad (56)$$

and

$$\begin{aligned} \epsilon(z) &\simeq \frac{c}{H_0\sqrt{\Omega_m}} \frac{l(z)}{a+k-1} \left(\frac{a-1}{a+\frac{11}{2}-\zeta} \right) n_A (1+z)^{3/2} \\ &\times \sigma_{\text{tot}}(E_0) \left(\frac{E_0}{E_1} \right)^k \left(\frac{E_1}{E_i} \right)^{a+k-1} \end{aligned}$$

$$\propto \epsilon_\delta(z) \times \left(\frac{E_0}{E_1} \right)^k \left(\frac{E_1}{E_i} \right)^{a+k-1}. \quad (57)$$

If we do not focus on the linear changed factors such as $(a-1)/(a+\frac{11}{2}-\zeta)$, mostly the power law spectrum will significantly increase the energy deposition $\epsilon(z)$ as well as the ionization rate $I(z)$ (and even a dramatic increase in some cases) by a factor of $(E_0/E_k)^k (E_1/E_i)^{a+k-1}$.

A black-body-like or say multicomponent spectral distribution $F(E, z) \propto E^b \exp(-dE)$ with a peak E_0 and $c > 0$ can be approximately written as $F(E, z) \propto x^b$ for $x < 1$ and $F(E, z) \propto \exp(-dx)$ for $x > 1$, where $x = E/E_0$. In this case we find the number density spectrum as

$$\begin{aligned} \frac{dn}{dE_\gamma} &\simeq \frac{cA}{H_0\sqrt{\Omega_m}} \frac{l(z)}{E_0 E_\gamma} \frac{(1+z)^{-3/2}}{\frac{11}{2}-b-\zeta} \\ &\times \left[\left(\frac{E_\gamma}{E_0} \right)^b + (f(d)-1) \left(\frac{E_\gamma}{E_0} \right)^{\frac{11}{2}-\zeta} \right], \end{aligned} \quad (58)$$

where A is an algebraic factor $A = [(1+b)^{-1} + d^{-1}]^{-1}$, and $0 < f(d) < 1$ can be obtained numerically, which is not important for the following discussion. The terms in number density spectrum are proportional to E_γ^b or $E_\gamma^{11/2-\zeta}$. According to equation (58), the integrated energy density $\epsilon(z)$ is expected to be similar as equation (52) for $b > k-1$. Otherwise the enhancement should be $\epsilon(z) \propto \epsilon_\delta(z) (E_0/E_1)^{k-b-1}$. A steep x^c with $c > 1$ for annihilation $k \sim 2$ and all the black-body-like SED for X-rays $k \simeq 0$, are more or less similar to the δ -function SED at E_0 .

Now we study the case of $E_X \ll 10$ keV for X-ray emission from very massive PBHs. Photon absorption in the IGM is important for $E_X \sim 1$ keV. The mean free path of X-ray photons describing by redshift change Δz as

$$\tau \sim \Delta z \frac{c}{H_0\sqrt{\Omega_m}} (1+z)^{-5/2} n_A (1+z)^3 \sigma_{\text{tot}}(1 \text{ keV}) \left(\frac{E_X}{1 \text{ keV}} \right)^{-k}, \quad (59)$$

or we have

$$\Delta z \sim 0.40 (1+z)^{-1/2} \left(\frac{E_X}{1 \text{ keV}} \right)^k, \quad (60)$$

where $k \simeq 3.3$ for the photonization cross section. Similarly as the former calculation, they energy density for a δ -function spectrum is

$$\epsilon_\delta(z) \sim \frac{0.40}{H_0\sqrt{\Omega_m}} l_{\text{acc}}(z) n_A \left(\frac{E_0}{1 \text{ keV}} \right)^k \sigma_{\text{tot}}(E_0). \quad (61)$$

Note that now we have a shallower density evolution $\epsilon_\delta(z) \propto (1+z)^3$ compared with the transparently propagation for the case of equation (54) as $\epsilon_\delta(z) \propto (1+z)^{\zeta+3/2}$. For a power law SED $F(E, z) \propto E^{-a}$ ($E_1 \leq E \leq E_2$), we obtain the energy density as

$$\begin{aligned} \epsilon(z) &\sim \frac{0.40c}{H_0\sqrt{\Omega_m}} l_{\text{acc}}(z) n_A \sigma_{\text{tot}}(E_0) \left(\frac{E_0}{1 \text{ keV}} \right)^k \left(\frac{E_1}{E_0} \right)^{a-1} \\ &\propto \epsilon_\delta(z) \left(\frac{E_1}{E_i} \right)^{a-1}. \end{aligned} \quad (62)$$

Therefore the energy density is enhanced for $E_1 > E_i$, but the enhancement is less significant compared with that of equation (57) for the same spectrum index a .

For a brief summary, the strength of UCMH radiation depends on its extended spectral energy distribution, which

will increase the properties of IGM ionization $I(z)$ and heating $\epsilon(z)$. Compared to the basic results with the monochromatic spectrum E_X for annihilation or E_X for X-ray emission, power law spectrum $\propto E^{-a}$ with $a > 0$ can increase the energy density effectively, but black-body-like spectrum is more like the monochromatic SED case. For locally heating $E_X \sim 1$ keV, the heating increases less significant than the transparently propagation case $\tau \ll 1$. Also, power law spectrum changes $\epsilon(z)$ and $I(z)$ more significant for annihilation than X-ray radiation.

5.4 More Massive UCMHs Inside First Dark Haloes

In Section 4 we assume that the number of UCMHs inside a dark halo is so huge that UCMHs in the halo are uniform distributed per halo mass $\frac{dn_{\text{UCMH}}}{dM_{\text{DM}}} = \text{const.}$ or per volume $\frac{dn_{\text{UCMH}}}{dV_{\text{DM}}} = \text{const.}$ This assumption can be invalid if the mass seed of a single UCMH m_h is comparable to $f_{\text{UCMH}} M_{\text{DM}}$. In this case the position of each UCMH is important to determine the energy deposition within the halo. Usually X-ray emission can be neglected in a massive UCMH due to photon trapping (Section 2.2.3), we only focus on the UCMH annihilation. Equation (49) in Section 4.2 is invalid for massive UCMHs $m_h \sim f_{\text{UCMH}} M_{\text{DM}}$. In this case $\epsilon_{\text{loc,iso}}$ in equation (49) should be calculated as the summation of individual UCMHs

$$\epsilon_{\text{loc,UCMH}}(z) = \frac{\sigma_{\text{tot}}(1-f_X)}{\mu m_p f_X} \sum_i \frac{L_{\text{UCMH},i} \rho(r_i)}{4\pi r_i^2}, \quad (63)$$

where $L_{\text{UCMH},i}$ and r_i are the annihilation luminosity and position of the i -th UCMH within the halo.

An extreme case is that there is only one massive UCMH inside a dark halo, the energy deposited in the gas at the center of the halo can be obtained by equation (63) in Section 4.1. Remember that for a uniformly distributed UCMHs with a same total mass of the single UCMH inside a halo we use equation (49). The ratio factor between (63) and (49) is

$$\begin{aligned} \text{factor} &= \left(\frac{R_{\text{core}}}{r_0} \right)^4 \left(\frac{3R_{\text{tr}}}{R_{\text{core}}} - 2 \right) \left[4 - \left(\frac{R_{\text{core}}}{r_{\text{tr}}} \right)^3 \right]^{-1} \\ &\simeq \frac{3}{4\xi} \left(\frac{R_{\text{core}}}{r_0} \right)^4, \end{aligned} \quad (64)$$

where r_0 is the location of the single massive UCMH from the halo center. If we take $R_{\text{core}} = \xi R_{\text{tr}}$ with $\xi \ll 1$, the factor can be approximately written as $(3/4\xi)(R_{\text{core}}/r_0)^4$. For a single UCMH located close to the isothermal case $r_0 \simeq R_{\text{core}}$, the factor (64) is $3/(4\xi)$. For a single UCMH located at the turnaround radius $r_0 \simeq R_{\text{tr}}$ equation (64) becomes $\simeq 3\xi^3/4$. Taking a typical value $\xi \sim 0.1$, the energy deposition ϵ_{loc} contributed by a single UCMH varies from ~ 10 higher to $\sim 10^{-3}$ lower compared to that contributed by the same total mass but uniformly distributed small UCMHs. Fig. 13 gives the gas x_{ion} and f_{H_2} inside a $10^6 M_\odot$ isothermal halo with a single UCMH located in difference locations. UCMH annihilation on the halo center will be less important for further located UCMH $> 2R_{\text{core}}$. The uniformly distributed UCMHs are more or less equivalent to a single UCMH located at approximately $\sim 1.5R_{\text{core}}$. As an example in this

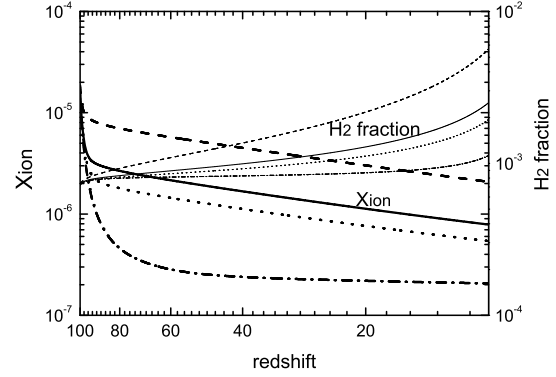


Figure 13. Ionization fraction x_{ion} (thick lines) and molecular hydrogen fraction H_2 (thin lines) in a $10^6 M_\odot$ isothermal halo with a single massive UCMH located at R_{core} (dashed lines), $2R_{\text{core}}$ (dotted lines) and $10R_{\text{core}}$ (dash-dotted lines) from the center of the halo. The solid lines shows the results given by many small UCMHs which number density is proportional to the halo density. Both single UCMH or small UCMHs is adopted a total UCMH fraction as $f_{\text{UCMH}} = 10^{-4}$, $z_{\text{vir}} = 100$ and $m_\chi c^2 = 10$ GeV.

figure, we take the UCMH fraction as $f_{\text{UCMH}} = 10^{-4}$ and $m_\chi c^2 = 10$ GeV. More massive dark matter particles or less UCMH fraction will give a faster decrease in energy deposition with the single UCMH moving outward the halo. We also check the importance of a single UCMH's position on the gas temperature inside a halo, but we see that the effect can be neglected for the temperature.

On the other hand, the energy deposition by a single UCMH compared with the volume uniformly distributed small UCMHs with a same total mass can be amplified by a factor

$$\begin{aligned} \text{factor} &\simeq \frac{1}{6} \left(\frac{R_{\text{core}}}{r_0} \right)^4 \left(\frac{R_{\text{tr}}}{R_{\text{core}}} \right)^3 \left(1 - \frac{R_{\text{core}}}{R_{\text{tr}}} \right) \\ &\simeq \frac{1}{6\xi^3} \left(\frac{R_{\text{core}}}{r_0} \right)^4, \end{aligned} \quad (65)$$

which gives an enhancement factor about $\sim 1/(6\xi^3) \sim 1/\xi^2$ for $r_0 = R_{\text{core}}$ and a weaker factor $\xi/6$ for $r_0 = R_{\text{tr}}$. These results show that the massive single UCMH is always more important for energy deposition compared with the volume uniformly distributed UCMHs.

Therefore we conclude that different UCMH distribution with a same total mass but different individual mass can change the energy deposition and structure evolution inside a halo. More concentrated distribution towards the halo center or a closer located single halo near the center gives a more significant effect on the gas ionization and heating at the halo center.

6 CONCLUSIONS

Ultracompact Minihaloes (UCMHs) have been proposed as the primordial dark matter structures which formed by dark matter accreting onto initial overdensity or primordial black holes (PBHs) after matter-radiation equality $z_{\text{eq}} \simeq 3100$

(Mack et al. 2007; Ricotti & Gould 2009). The key difference between UCMHs and the first dark halo structures is that, UCMHs are seeded by primordial density perturbations produced in the very early Universe such as the phase transition epoches ($10^{-3} \leq \delta \leq 0.3$ for the initial overdensity or $\delta > 0.3$ for PBHs), so they can grow shortly after $z \sim z_{\text{eq}}$. The radiation from UCMHs in the early Universe includes dark matter annihilation from all UCMHs, and X-ray emission from gas accretion onto PBHs. In this paper we investigate the influence of UCMH radiation on the early ionization and thermal history of the intergalactic medium, and the following evolution of the first massive baryonic objects. Our conclusions are as follows.

1. UCMH annihilation can totally dominate over the homogenous dark matter background annihilation, and provide a new gamma-ray background even for a tiny UCMH fraction $f_{\text{UCMH}} = \Omega(z_{\text{eq}})/\Omega_{\text{DM}} \sim 2.2 \times 10^{-15} m_{\chi,100}^{-2/3} (1+z)^2$ with $m_{\chi,100} = m_{\chi} c^2 / 100$ GeV. We conclude that the influence of dark matter annihilation on the IGM evolution can be significantly enhanced when we include UCMHs besides the homogenous dark matter background. In most cases the UCMH annihilation had been the dominated sources of ionization and heating gas since matter-radiation equality epoch, until the X-ray emission from PBHs or large scale structure formation become important at $z \leq 100$.

2. The impact of UCMH annihilation on the IGM can be approximately estimated by the quantity $m_{\chi,100}^{-1} f_{\text{UCMH}}$. The threshold of UCMH abundance f_{UCMH} to affect the IGM evolution by dark matter annihilation is $m_{\chi,100}^{-1} f_{\text{UCMH}} > 10^{-6}$. After matter-radiation equality epoch, the IGM ionization fraction x_{ion} can be increased from $x_{\text{ion}} \sim 10^{-4}$ in the absence of any energy injections to an upper bound $x_{\text{ion}} \sim 0.1$, and the IGM temperature from the adiabatic cooling $T_{\text{m}} \propto (1+z)^2$ to a maximum value $T_{\text{m}} \sim 5000$ K for the upper bound case $m_{\chi,100}^{-1} f_{\text{UCMH}} \sim 10^{-2}$, which is constrained using the CMB optical depth at late times $z < 30$. UCMH annihilation is able to significantly increase the Thomson optical depth $\tau \geq 0.1$ in the early Universe $z \gg 30$, which is unrelated with the measured CMB optical depth at $z < 30$. The UCMH annihilation luminosity is based on the UCMH profiles, where we take $\rho \propto r^{-2.25}$ from literature (Bertschinger 1985), steeper (shallower) profiles decrease (increase) the allowed upper limit of f_{UCMH} , but the variations of the overall IGM chemical and thermal quantities should not be changed too much, because the fraction of UCMHs with a profile $\rho \propto r^{-1.5}$ as the PBH hosts are very small, and $\rho \propto r^{-3}$ occurs only in the halo outskirts $r \gg r_{\text{cut}}$.

3. Each PBH is located in its host UCMH (Mack et al. 2007). We emphasize that the impact of X-ray emission from PBH host UCMH systems is limited by the low abundance of PBHs ($f_{\text{PBH}} \ll f_{\text{UCMH}}$), the average inefficient radiation ($\eta \ll 1$), the photon trapping effect by the accreted baryons in host UCMHs, and outflows produced by rapid accretion feedback. Sufficient massive host UCMHs can accrete and thermalize the infalling baryons, which are accumulated inside the UCMHs with a mass fraction of the UCMH $f_b > 10^{-3}$, and trap X-rays from the accreting PBHs until a critical redshift $z_m \sim 32(\delta m/M_{\text{PBH}})^{1/2} m_{\chi,100}^{-5/12}$, below which X-rays from a super-Eddington accretion flows onto PBHs could escape the surrounding baryon environ-

ment in the host UCMHs. Although the PBH abundance is $f_{\text{PBH}} \ll f_{\text{UCMH}}$ due to the much higher perturbation threshold for the PBH formation, X-ray emission could dominate over UCMH annihilation and become more promising cosmic energy source of the IGM ionization and heating at $z < z_m$ if the PBH abundance is above a threshold $\eta f_{\text{PBH}}/f_{\text{UCMH}} \sim 3.1 \times 10^{-8} m_{\chi,100}^{-4/3} (1+z)$, which is only allowed beyond the standard Gaussian density perturbation scenario.

4. As UCMHs are expected to exist in our Galaxy, we expect that UCMHs collapse with the homogenous dark matter background to form the first large scale dark matter objects (dark haloes). If this is the case, the dark matter annihilation from UCMHs inside the first dark halo still dominates over the extended dark matter annihilation background inside the halo even after the halo virialization. UCMH radiation, including both dark matter annihilation and accretion emission, can dramatically suppress the formation of the low mass first baryonic structure, since UCMH radiation heats the IGM and provide a hot ambient gas environment up to $T_{\text{m}} \sim 10^4$ K. The UCMH radiation enhances the baryon chemical quantities such as x_{ion} and f_{H_2} by orders of magnitude from $x_{\text{ion}} \sim 10^{-6}$ and $f_{\text{H}_2} \sim 10^{-4}$ to the upper bound of $x_{\text{ion}} \sim 10^{-4}$ and $f_{\text{H}_2} \sim 5 \times 10^{-3}$. However, the impact of UCMH radiation on the baryon temperature of the first baryonic objects is very small, which shows that the influence of UCMH radiation on the temperature of first baryonic objects is small compared to the molecular hydrogen cooling and virialization time z_{vir} . However, the higher abundant x_{ion} and f_{H_2} provided by UCMH radiation decrease the gas temperature in the later gas collapse phase and can produce lower fragmentation mass scale and lower mass first stars.

Also, we point out that, different spectral energy distributions of UCMH radiation also affect the processes of ionizing radiation and heating gas. More concentrated UCMH distribution within a dark matter halo provides a more promising ionization phenomenon of the gas in first dark haloes. UCMHs should be distinguished from the small dark structure which formed during the structure formation epoch after $z \sim 100$. Future work need to be done to investigate the importance of small dark matter structure down to the earth mass compared with UCMH radiation in the early Universe at $z \sim 60$. Also, the CMB polarization anisotropies, 21 cm spectrum and Compton y-parameter affected by the UCMH radiation also need to be further studied for a better constraint on the UCMH abundance.

ACKNOWLEDGMENTS

DZ is grateful to John Beacom and Brain Lacki for stimulating discussions and useful comments on the manuscript. He would also like to thank David Weinberg and Alexander Belikov for helpful discussions on the baryonic fraction within dark haloes and dark halo structure formation history. Furthermore, he acknowledges Todd Thompson and Zi-Gao Dai.

APPENDIX A: PROFILES OF FIRST DARK STRUCTURE

The dark matter profile we use in this paper are as follows. Most of the equations list below can be found in Tegmark et al. (1997), Ripamonti (2007) and Ripamonti et al. (2007a). A dark matter halo with a mass M_{DM} is assumed to distribute inside a truncation radius R_{tr} , which is given by

$$R_{\text{tr}}(z, z_{\text{vir}}) = \begin{cases} \left[\frac{3}{4\pi} \frac{M_{\text{DM}}}{\rho_{\text{th}}(z)} \right]^{1/3} & z \geq z_{\text{ta}} \\ R_{\text{vir}} \left[2 - \frac{t(z) - t(z_{\text{ta}})}{t(z_{\text{vir}}) - t(z_{\text{ta}})} \right] & z_{\text{vir}} \leq z \leq z_{\text{ta}} \\ R_{\text{vir}} & z \leq z_{\text{vir}} \end{cases} \quad (\text{A1})$$

Here z_{vir} is the redshift of halo virialization, $z_{\text{ta}} \simeq 1.5(1 + z_{\text{vir}}) - 1$ is the turnaround redshift. The dark matter mass inside the halo M_{DW} is given as a parameter here. Dark matter within the halo is assumed to distribute uniform at $z > z_{\text{ta}}$ with a density evolution

$$\rho_{\text{th}}(z, z_{\text{vir}}) = \rho_{\text{DM}}(z) e^{1.9A/(1-0.75A^2)}, \quad (\text{A2})$$

where $A(z) = (1 + z_{\text{vir}})/(1 + z)$. The virial radius R_{vir} is given by

$$R_{\text{vir}} = \frac{1}{2} R_{\text{tr}}(z_{\text{ta}}) = \frac{1}{2} \left[\frac{3}{4\pi} \frac{M_{\text{DM}}}{\rho_{\text{th}}(z_{\text{ta}})} \right]^{1/3}. \quad (\text{A3})$$

For an isothermal halo profile with a core radius R_{core} inside R_{tr} , the dark matter density $\rho(z)$ is a constant ρ_{core} for $r \leq R_{\text{core}}$, $\rho(z) \propto r^{-2}$ for $R_{\text{core}} \leq r \leq R_{\text{tr}}$. The density goes to the background dark matter density for $r > R_{\text{tr}}$. Here the core radius R_{core} is obtained as

$$R_{\text{core}}(z, z_{\text{vir}}) = \begin{cases} R_{\text{tr}}(z) & z \geq z_{\text{ta}} \\ R_{\text{vir}} \left[2 - (2 - \xi) \frac{t(z) - t(z_{\text{ta}})}{t(z_{\text{vir}}) - t(z_{\text{ta}})} \right] & z_{\text{vir}} \leq z \leq z_{\text{ta}} \\ \xi R_{\text{vir}} & z \leq z_{\text{vir}} \end{cases} \quad (\text{A4})$$

where the coefficient ξ is introduced as a parameter. And ρ_{core} can be obtained integrating the halo mass within R_{tr} as M_{DM} . The total luminosity produced by the annihilation of dark matter particles distributed within the isothermal halo is

$$L_{\text{ext,iso}} = \frac{2\pi\rho_{\text{core}}^2}{m_{\chi}} \langle \sigma v \rangle c^2 R_{\text{core}}^2 \left(R_{\text{tr}} - \frac{2}{3} R_{\text{core}} \right). \quad (\text{A5})$$

On the other hand, the widely used NFW dark matter profile is $\rho(r) \propto r^{-1}(1+r/R_{\text{core}})^{-1}$ for $r \leq R_{\text{tr}}$. Similarly we can write down the complete formula of density distribution as the function of redshift, and the luminosity produced by dark matter annihilation.

The virial temperature of a halo T_{vir} is calculated as

$$T_{\text{vir}} = \frac{\mu m_p}{2k_B} \frac{GM_{\text{DM}}}{R_{\text{vir}}}, \quad (\text{A6})$$

sometimes people use the total mass M_{halo} instead $M_{\text{DM}} f_{\chi}$. However, as we consider if the gas from the background can collapse into the halo, we adopt the pure dark halo mass as to calculate the initial virial temperature. Therefore we can obtain the virial temperature as $T_{\text{vir}} = 8.2 \times 10^{-3} \text{ K} (1 + z_{\text{vir}})(M_{\text{DM}}/M_{\odot})^{2/3}$, or $T_{\text{vir}} = 380 \text{ K} (M_{\text{DM}}/10^4 M_{\odot})^{2/3}(1 + z_{\text{vir}})/100$. The baryon falling can occur when the IGM temperature T_{m} around the halo to be $T_{\text{m}} < T_{\text{vir}}$, otherwise the gas pressure will impede the gas falling into the halo and

collapsing to form smaller structure. Moreover, the condition $T_{\text{CMB}} = T_{\text{vir}}$ with $T_{\text{CMB}} = 2.73 \text{ K} (1 + z_{\text{vir}})$ gives a critical halo mass $M_{\text{DM}} = 6.1 \times 10^3 M_{\odot}$.

REFERENCES

- Abolmasov P., Karpov S., Kotani T., 2009, PASJ, 61, 213
 Abramowicz M. A., Czerny B., Lasota J. P., Szuszkiewicz E., 1988, ApJ, 332, 646
 Abramowicz M. A., Fragile P. C., 2011, arXiv: 1104.5499
 Abramowicz M. A., Jaroszyński M., Sikora, M., 1978, A&A, 63,221
 Abazajian K., Fuller G. M., Patel M., 2001, Phys. Rev. D., 64, 023501
 Abdo A. A., et al. 2009, Phys. Rev. Lett., 102, 181101
 Abel T., Bryan G. L., Norman M. L., 2002, Science, 295, 93
 Aharonian F., et al. 2008, Phys. Rev. Lett., 101, 261104
 Bambi C., et al. 2009, MNRAS, 399, 1347
 Barkana R., Loeb A., 2007, Rep. Prog. Phys., 70, 627
 Barrow J. D., Silk J., 1979, Gen. Relativ. Gravitation, 10, 633
 Becker R. H., et al. 2001, ApJ, 122, 2850
 Belikov A. V., Hooper D., 2009, Phys. Rev. D., 80, 035007
 Belikov A. V., Hooper D., 2010, Phys. Rev. D., 81, 043505
 Belotsky K. M., Khlopov M. Y., Legonkov S. V., Shibaev K. I., 2005, Gravitation and Cosmology 11, 27
 Bergström L., Ullio P., Buckley H., 1998, Astropart. Phys., 9, 137
 Bertschinger E., 1985, ApJS, 58, 39
 Biermann P. L., Kusenko A., 2006, Phys. Rev. Lett., 96, 1301
 Blandford, R. D., Begelman, M. C., 1999, MNRAS, 303, L1
 Boehm C., Mathis H., Devriendt J., Silk J., 2005, MNRAS, 360, 282
 Bromm V., Yoshida N., Hernquist L., McKee C. F., 2009, Nature, 459, 49
 Bullock, J. S., Primack, J. R., 1997, Phys. Rev. D., 55, 7423
 Carr B. J., 1981, MNRAS, 194, 639
 Carr B. J., Hawking S. W., 1974, MNRAS, 168, 399
 Carr, B. J., Kohri, K., Sendouda, Y., Yokoyama, J., 2010, Phys. Rev. D., 81, 104019
 Cen R., 2003, ApJ, 591, 12
 Chang J., et al. 2008, Nature, 456, 362
 Chen X.-L., Kamionkowski M., 2004, Phys. Rev. D, 70, 043502
 Chluba J., 2010, MNRAS, 402, 1195
 Chuzhoy L., 2008, ApJ, 679, L65
 Ciardi B., Scannapieco E., et al. 2006, MNRAS, 366, 689
 Cirelli M., Iocco F., Panci P., 2009, J. Cosmology Astropart. Phys., 10, 9
 Dunkley J., et al. 2009, ApJS, 180, 306
 Diemand J., Moore, B., Stadel, J., 2005, MNRAS, 364, 665
 Feng J. L., Matchev K. T., Wilczek F., 2001, Phys. Rev. D., 63, 045024
 Fan X., et al. 2002, ApJ, 123, 1247
 Frampton P. H., Kawasaki M., Takahashi F., Yanagida T. T., 2010, J. Cosmol. Astropart. Phys. 04, 023
 Galli S., Iocco F., Bertone G., Melchiorri A., 2009, Phys. Rev. D., 80, 3505

- Galli D., Palla F. 1998, *A&A*, 335, 403
- Gnedin N. Y., Ostriker J. P., Rees M. J. 1995, *ApJ*, 438, 40
- Green, A. M., Liddle, A. R. 1997, *Phys. Rev. D.*, 56, 6166
- Green, A. M., Liddle, A. R., Riotto, A. 1997, *Phys. Rev. D.*, 56, 7559
- Green A. M., Hofmann S., Schwarz D. J. 2005, *JCAP*, 08, 003
- Haiman Z., Loeb A., 1997, *ApJ*, 483, 21
- Hansen S. H., Haiman Z., 2004, *ApJ*, 600, 26
- Hawking S., 1971, *MNRAS*, 152, 75
- Heger A., Woosley S. E., 2002, *ApJ*, 567, 532
- Hoeft M., Yepes G., Gottlöber S., Springel, V., 2006, *MNRAS*, 371, 401
- Hollenbach D., McKee C. F., 1979, *ApJS*, 41, 555
- Hooper D., Kaplinghat M., Strigari L. E., Zurek K. M., 2007, *Phys. Rev. D.*, 76, 3515
- Iliev I. T., Scannapieco E., Shapiro P. R., 2005, *ApJ*, 624, 491
- Igumenshchev I. V., Narayan R., Abramowicz M. A., 2003, *ApJ*, 592, 1042
- Ishiyama T., Makino J., Ebisuzaki E., 2010, *ApJL*, 723, 195
- Josan A. S., Green A. M., 2009, *Phys. Rev. D.*, 79, 103520
- Josan A. S., Green A. M., 2010, *Phys. Rev. D.*, 82, 083527
- Kanzaki T., Kawasaki M., Nakayama K., 2010, *Prog. Theor. Phys.*, 123, 853
- Kohri K., Narayan R., Piran T., 2005, *ApJ*, 629, 341
- Komatsu E., et al. 2009, *ApJS*, 180, 330
- Lacki B. C., Beacom J. F. 2010, *ApJL*, 720, 67
- Lidsey J. E., Carr B. J., Gilbert J. H., 1995, *Nucl. Phys. Proc. Suppl.*, 43, 75
- Mack K. J., Ostriker J. P., Ricotti M., 2007, *ApJ*, 665, 1277
- Mack K. J., Wesley D. H., arXiv: 0805.1531
- Madau P., et al. 2004, *ApJ*, 604, 484
- Mapelli M., Ferrara A., 2005, *MNRAS*, 364, 2
- Mapelli M., Ferrara A., Pierpaoli E., 2006, *MNRAS*, 375, 1399
- Meiksin A. A., 2009, *Rev. Mod. Phys.*, 81, 1405
- Miller M. C., Ostriker E. C., 2001, *ApJ*, 561, 496
- Milosavljević M., Couch S. M., Bromm, V. 2009, *ApJL*, 696, 146
- Milosavljević M., Bromm, V., Couch, S. M., Oh, S. P. 2009, *ApJ*, 698, 766
- Myers Z., Nusser A., 2008, *MNRAS*, 384, 727
- Narayan R., Yi, I., 1994, *ApJ*, 428, L13
- Narayan, R., Igumenshchev, I. V., Abramowicz, M. A., 2000, *ApJ*, 539, 798
- Narayan R., Mahadevan R., Quataert E., 1998, in Abramowicz M. A., Bjornsson G., Pringle J. E., eds, *Theory of Black Hole Accretion Disks*. Cambridge Univ. Press, Cambridge, p. 148
- Natarajan A., Schwarz D. J., 2008, *Phys. Rev. D.*, 78, 103524
- Natarajan A., Schwarz D. J., 2009, *Phys. Rev. D.*, 80, 043529
- Natarajan A., Schwarz D. J., 2010, *Phys. Rev. D.*, 81, 123510
- Oda T., Totani T., Nagashima M., 2005, *ApJ*, 633, 65L
- Okamoto T., Gao L., Theuns T., 2008, *MNRAS*, 390, 920
- Park K. H., Ricotti, M. 2011, arXiv: 1006.1302
- Padmanabhan N., Finkbeiner D. P., 2005, *Phys. Rev. D.*, 72, 023508
- Poutanen J., Lipunova G., Fabrika S., Butkevich A. G., Abolmasov P., 2007, *MNRAS*, 377, 1187
- Press W. H., Schechter P., 1974, *ApJ*, 187, 425
- Pierpaoli E., 2004, *Phys. Rev. Lett.*, 92, 031301
- Ricotti M., 2007, *ApJ*, 662, 53
- Ricotti M., Gould A., 2009, *ApJ*, 707, 979
- Ricotti M., Ostriker J. P., 2004, *MNRAS*, 350, 539
- Ricotti M., Ostriker J. P., 2004, *MNRAS*, 352, 547
- Ricotti M., Ostriker J. P., Gnedin N. Y., 2005, *MNRAS*, 357, 207
- Ricotti M., Ostriker J. P., Mack K. J., 2008, *ApJ*, 680, 829
- Ripamonti E., 2007, *MNRAS*, 376, 709
- Ripamonti E., Mapelli M., Ferrara A., 2007, *MNRAS*, 374, 1067
- Ripamonti E., Mapelli M., Ferrara A., 2007, *MNRAS*, 375, 1399
- Ripamonti E., Mapelli M., Zaroubi S., 2008, *MNRAS*, 387, 158
- Rybicki G. B., Lightman A. P., *Radiative Processes in Astrophysics*, 2004, Wiley-VCH, New York
- Salvaterra R., Haardt F., Ferrara A., 2005, *MNRAS*, 362L, 50
- Sandick P., Diemand J., Freese K., Spolyar D., 2011, *JCAP*, 01, 018
- Saito R., Shirai S., 2011, *Phys. Lett. B.*, 697, 95
- Saito R., Yokoyama J., Nagata, R. 2008, *J. Cosmol. Astropart. Phys.*, 06, 024
- Sazonov S. Y., Ostriker J. P., Sunyaev R. A., 2004, *MNRAS*, 347, 144
- Scott P., Sivertsson S., 2009, *Phys. Rev. Lett.*, 103, 211301
- Seager S., Sasselov D. D., Scott D., 2000, *ApJ*, 128, 407
- Shakura N. I., Sunyaev R. A., 1973, *A&A*, 24, 337
- Shapiro S. L. 1973a, *ApJ*, 180, 531
- Shapiro S. L. 1973b, *ApJ*, 185, 69
- Sheth, R. K., Tormen, G., 1999, *MNRAS*, 308, 119
- Shull J. M., van Steenberg M. E., 1985, *ApJ*, 298, 268
- Shull J. M., Venkatesan A., 2008, *ApJ*, 685, 1
- Slatyer T. R., Padmanabhan N., Finkbeiner D. P., 2009, *Phys. Rev. D*, 80, 3526
- Smith N., Owocki S. P., 2006, *ApJL*, 645, 45
- Spolyar D., Freese K., Gondolo P., 2008, *Phys. Rev. Lett.*, 100, 051101
- Spolyar D., Freese K., Gondolo P., 2009, *ApJ*, 705, 1031
- Stacy A., Bromm V., 2007, *MNRAS*, 382, 229
- Stasielak J., Biermann P. L., Kusenkov A., 2007, *ApJ*, 654, 290
- Tashiro H., Sugiyama N., 2006, *MNRAS*, 368, 965
- Tegmark M., et al. 1997, *ApJ*, 474, 1
- Thomas R. M., Zaroubi S., 2008, *MNRAS*, 384, 1080
- Ullio P., Bergström J., Edsjö J., Lacey, C., 2002, *Phys. Rev. D* 66, 123502
- Khlopov M. Y., 2010, *RAA*, 10, 495
- Volonteri M., Gnedin N., 2009, *ApJ*, 703, 2113
- Wang J.-M., Chen, Y.-M., Hu C., 2006, *ApJL*, 637, 85
- Whalen D., Hueckstaedt R. M., McConkie T. O., 2010, *ApJ*, 712, 101
- Weymann R., 1965, *Phys. Fluids*, 8, 2112
- Wise J. H., Abel T., 2008, *ApJ*, 684, 1
- Wyithe S., Loeb A., 2003, *ApJ*, 588, L69
- Yoshida N., 2009, arXiv: 0906.4372

- Yoshida N., Omukai K, Hernquist L., Abel T., 2006, ApJ, 652, 6
Yuan Q., et al. 2010, JCAP, 1010,023
Zdziarski A., Svensson R., 1989, ApJ, 344, 551
Zhang L., Chen X.-L., Lei Y.-A., Si Z.-G., 2006, Phys. Rev. D., 74, 103519